Modern NMR methods for advanced materials characterization

Thesis summary

PhD: Dumitrița Moldovan
Scientific master: Professor Dr. Dan Eugen Demco

Keywords

EPDM, elastomers, filler, Payne effect, cross-link natural rubber, biopolymers, α keratin, NMR ^{1}H, 1D and 2D pulse sequence, CPMG, Hahn echo, double quantum curves, DQ, saturation recovery curves, spin-lock, transverse relaxation time, longitudinal relaxation time, correlation time, residual second moment, molecular exchange process, magnetization exchange process, storage time, exchange time, the distribution of NMR parameters, Monte-Carlo, Laplace transform, Fourier transform, residual dipolar Hamiltonian, residual dipolar coupling.

Contents

Introduction

Nuclear magnetic resonance is one of most frequently used by spectroscopy methods used in chemistry, used for determination of molecular structure and dynamics for simply to the complex molecules. Local diversity plays an essential role in the development of new materials with improved properties. In particular, the Nano-composite elastomers are important materials extensively used in the rubber industry. Due to their demanding applications, such materials must fulfill many requirements.

The aim of this thesis is to developed new nuclear magnetic resonance methods for studying advance materials. Among these materials, for this study was choose three types of different materials like: natural rubber with different vulcanization degree, elastomers with fillers and α keratin by biopolymers categories. Like a novelty was introduced for the first time Payne effect for characterization of specific EPDM with fillers, this material have a viscoelastic properties, the data being processed with the help of invers Laplace transform.

In the chapters four and five heterogeneity elastomers reinforced with different fillers are emphasized by the distribution of relaxation times, T_1, T_2, $T_{1\rho}$, second residual van Vleck moments, M_2 and correlation times τ_c. These distributions were measured by different NMR methods in function of specific parameters. Interpretation of experimental data and characterization of Nano-composite elastomer properties was done using a computer algorithm based on inverse Laplace transform, is another point of novelty.

In chapter six we used several NMR double quantum experiments to characterize the effect of aging of natural rubber and elastomers reinforced characterize heterogeneity. Aging effects were observed by the appearance of two peaks in the double quantum curves interpreted as a bimodal distribution of proton dipole couplings waste of polymer chains. For the first time analysis of such experimental curves measured by two quanta of signal was performed using Fourier transform. Increase curves of two quanta and decrease curves were recorded over several years for a series of samples with different densities of natural rubber cross-link.

In seven chapters discussed the essence of spins and diffusion experiments were performed by spin diffusion experiments to understand the morphology of reinforced elastomers and α keratin fibrils hydrated. These experiments of spin diffusion involve observing the diffusion that affects the transport parameters of nuclear spins. For the first time using inverse Laplace transform with complex kernel to identify different phases of

EPDM elastomers reinforced with fillers, the kernel is compose by a exponential function and a Abragamian function.

The last chapter presents ultra-fast molecular exchange processes performed poorly so far in the literature. To understand and interpret the correlation maps of T_2-T_2 in the presence of molecular exchange was created a Monte Carlo simulation program is described in this chapter. In the last part for the first time were recorded instead of magnetization processes for samples vulcanized natural rubber and elastomer reinforced with fillers

Ideas and discussions in this thesis have been completed with five articles published in specialized international magazines and three ISI in training, also with participation in international conferences. This thesis developed a topic with current flair and modern, remaining open to continue research in this field and after completing this work.

Some experimental results of the thesis

Chapter 3 Characterization of nanocomposit polymers

3.3 Filler properties

EPDM (ethylene-propylene-diene terpolymers) and related compounds with these are the most popular among elastomers. Thereby at the same concentration of fillers, the differences in product properties are dominated by the specific filler-filler interaction and the interaction between filler surface and polymer chains. One of the most used Nano-filler is carbon black (CB), another type used in this thesis is based on silicon and third class of fillers is based on calcium carbonate [1-13].

Table 3.1. The characteristics of carbon black fillers. The STSA represents the statistical thickness surface area, BET is related to nitrogen adsorption and CTAB is the cethyl-trimethyl-ammonium bromide adsorption methods. The percolation threshold was measured by electrical resistance method.

Filler type	Average particle size [nm]	Surface area [m^2/g]			Percolation threshold [phr]
		STSA	BET	CTAB	
N121	28	115	118	117	20 ÷ 40
Ecorax® 1720	47	115	123	116	20 ÷ 40
N683	73	34	36	40	60 ÷ 70
N990	254	7.1	7.8	8.3	> 70

3.4 Viscoelastic character of reinforced elastomers shown by Payne effect

The enhancement of elastomers by incorporation of fillers can best be studied by the increase of the elastic modulus and viscosity beyond the values of the polymer matrix. The accepted explanation for the filler reinforcement mechanism is based on the filler/filler associations formed during sample preparation. This problem is not trivial and was discussed extensively in [7]. The complex shear modulus $G=G'+iG''$ is the quantity used to determinate the viscoelastic properties of elastomers. The storage modulus G' depends on the strain, and decays with increasing shear-strain amplitude. This strain softening behavior is known as the Payne effect. There are several models that can provide a good quantification of the Payne effect, like the Kraus model, the viscoelastic model, cluster-cluster aggregation model, etc. Moreover, a strain memory effect is observed in the stress/strain curves which give rise to a hysteresis. In the present work we will focus on the quantification of the Payne effect in terms of the decay of G' with increasing shear strain γ_0 (see fig. 3.9) [7].

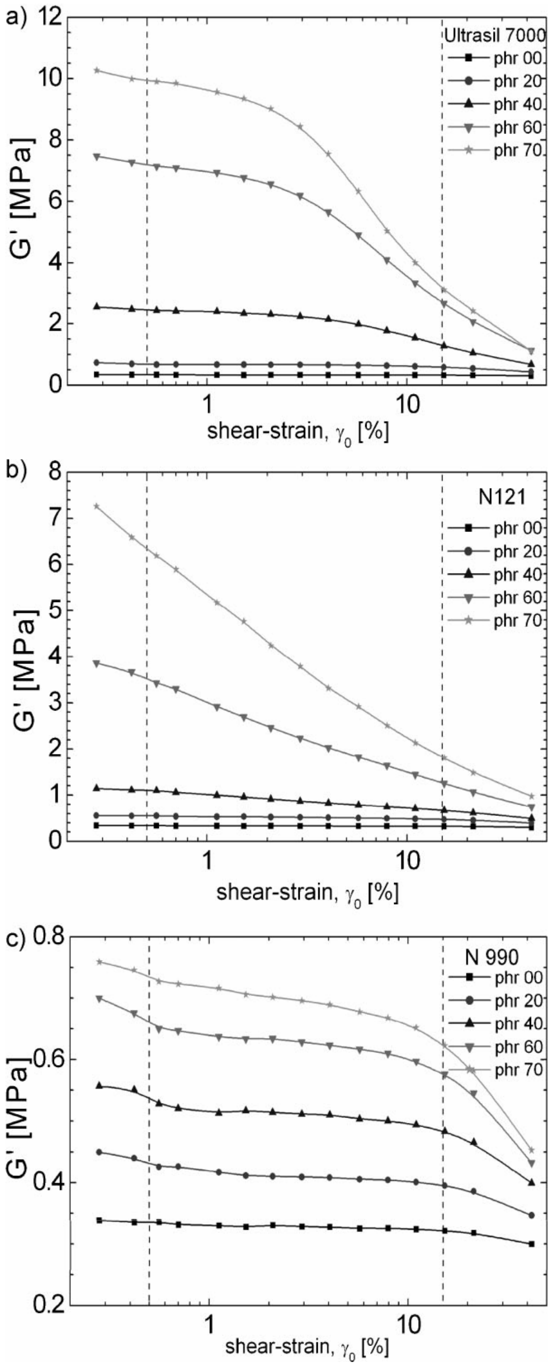

Fig. 3.9 Dependencies of the real part of the shear modulus (storage modulus) G' on the percent strain values for different filler contents: 0 (unfilled), 20, 40, 60 and 70 phr for (a) Ultrasil® 7000 GR, (b) N121, and (c) N990 filler types. The vertical dashed lines show the 0.5 and 15% strain values used to evaluate the Payne effect.

Quantitative characterization of the Payne effect

The Payne effect can be quantified from experimental data by considering the ratio between the storage modulus recorded at 15 % strain amplitude to the value of shear modulus recorded at 0.5 % strain amplitude,

$$P_e = \frac{G'(\gamma_0 = 15\%)}{G'(\gamma_0 = 0.5\%)}. \tag{3.2}$$

At this point, we would like to introduce another quantity that can describe the Payne effect. It takes into account the increase of the shear modulus due to filler/filler interactions with respect to the shear-strain amplitude range. This quantity is related to the slope in the logarithmic,

$$P(\gamma_{0,1}, \gamma_{0,2}) = \frac{\log\left\{G'_{\mathrm{f}}(\gamma_{0,2}) - G'_{\mathrm{uf}}(\gamma_{0,2})\right\} - \log\left\{G'_{\mathrm{f}}(\gamma_{0,1}) - G'_{\mathrm{uf}}(\gamma_{0,1})\right\}}{\gamma_{0,2} - \gamma_{0,1}}, \tag{3.3}$$

where $\gamma_{0,1}$ and $\gamma_{0,2}$ are particular domain limits of the shear-strain, $\mathrm{G}'_{\mathrm{uf}}$ is the storage modulus of the unfilled EPDM sample and G'_{f} is the storage modulus of the filled elastomer. The use of this quantity to characterize the filler/filler interactions related to the Payne effect. The dependence of the storage modulus G' on the shear strain amplitude for the EPDM samples filled at 70 phr was investigated (fig 3.10).

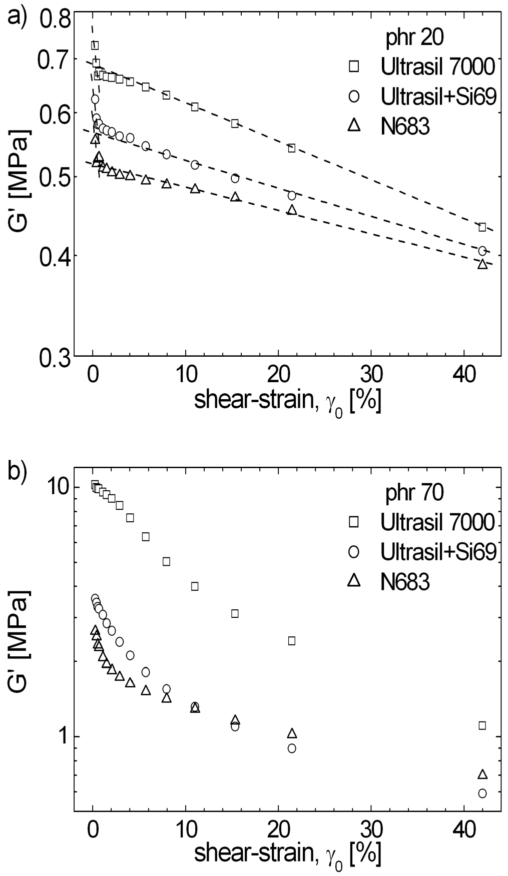

Fig. 3.10 Measured storage modulus G', versus strain γ_0 for EPDM filled with Ultrasil® 7000 GR, Ultrasil® 7000 GR + Si69, and N683 at a) 20 phr si b) 70 phr filler content. The straight line in a) are the best fits for small and large strain values γ_0.

Evaluations of Payne effect using the empirical quantity $P(\gamma_{0,1}, \gamma_{0,2})$ defined in Eq. (3.3) as function of filler content are shown in Fig. 3.11b for EPDM rubber reinforced with carbon black filler and in Fig. 3.11c for EPDM rubber reinforced with silane and precipitated calcium carbonate based fillers, where $\gamma_{0,1} = 0.005$ and $\gamma_{0,2} = 0.15$ corresponding to the 0.5 % and 15 % (see eq. 3.3).

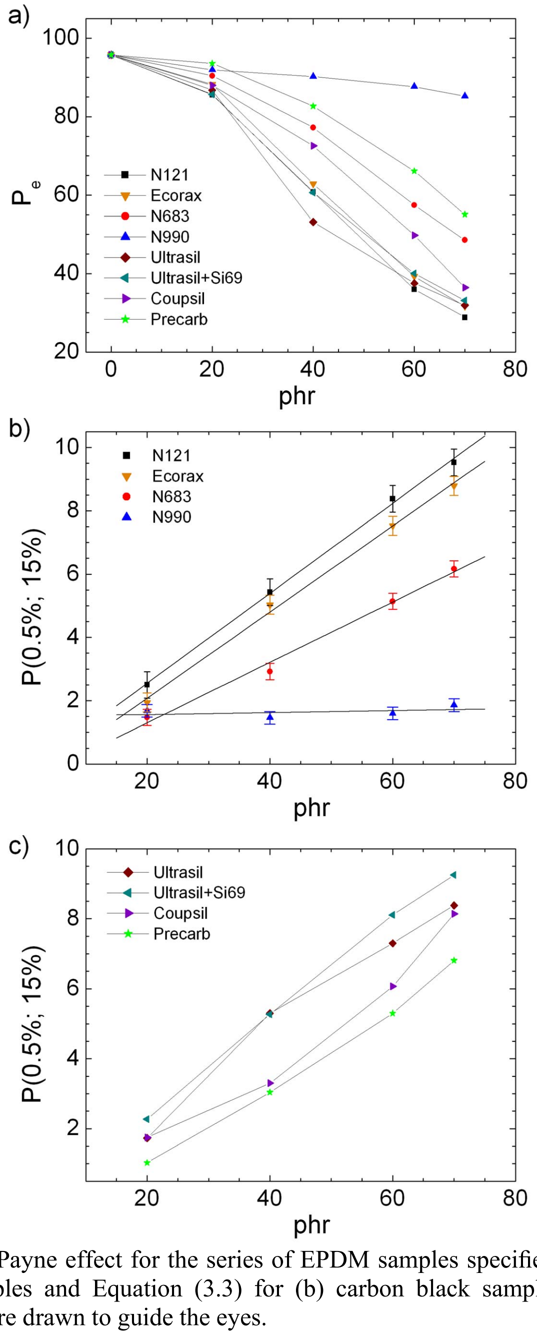

Fig. 3.11 The evaluation of Payne effect for the series of EPDM samples specified in Table 1 according to (a) Equation (3.2) for all samples and Equation (3.3) for (b) carbon black samples and (c) non-carbon-black samples. The straight lines are drawn to guide the eyes.

Heterogeneity of the Payne Effect by Laplace Inversion

In the following the complex Payne decay functions of Figs. 3.9 are analyzed in terms of a distribution function $f(\gamma_c)$ of critical shear-strain constants, i.e.,

$$G'(\gamma_0) = \int_0^\infty f(\gamma_c) \exp\left\{-\frac{\gamma_0}{\gamma_c}\right\} d\gamma_c \ . \tag{3.6}$$

The above relationship can be regarded as a Laplace transform. Smallest values of critical shear-strain γ_c, and large slopes in the Payne decay curves, can be associated with weak filler-filler interactions, while large γ_c values can be associated with strong filler-filler interactions. Inverse Laplace transformation algorithms, can be applied successfully to obtain the distribution function $f(\gamma_c)$. It relates to the heterogeneity of the filler-filler interaction. Peaks in the distribution $f(\gamma_c)$ can be qualified both in terms of peaks center of gravity of γ_c and the width of the distribution.

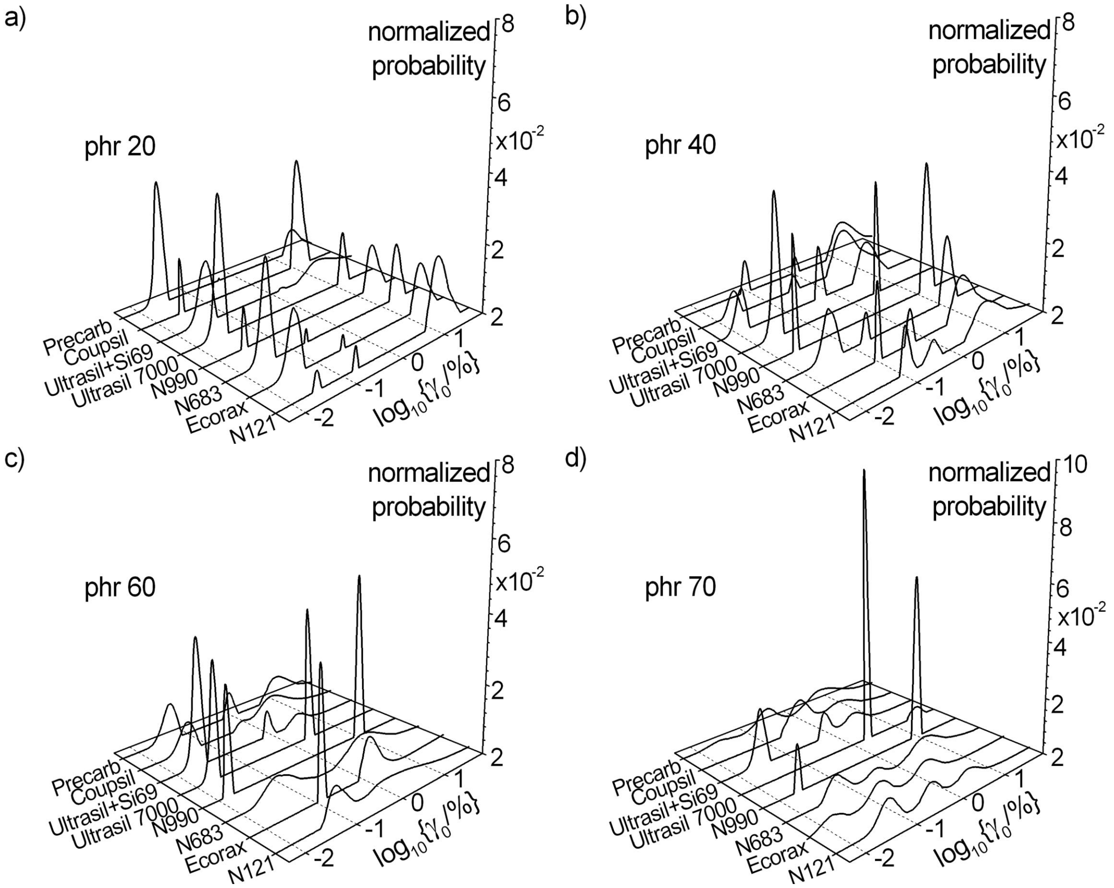

Fig. 3.12 Normalized probabilities obtained from Laplace inversions of strain-stress curves for the series of filled EPDM samples for (a) 20 phr (b) 40 phr (c) 60 phr, and (d) 70 phr filler content.

3.5 Cross-link natural rubber

Tabel 3.3 Properties series of samples cross-linked natural rubber.

Sample	Sulf acceleration content (phr)	Shear strain modulus G (dNm)	Young modulus E(MPa)
NR1	1-1	5.2	0.9
NR2	2-2	8.5	1.5
NR3	3-3	11.2	2.0
NR4	4-4	13.2	2.1
NR5	5-5	14.5	2.2
NR6	6-6	15.4	2.4
NR7	7-7	16.2	2.8

**Fitting errors were smallest than 10%.

Chapter 4. Heterogeneity of polymeric chain dynamics shown by relaxation times distribution

An important role in characterizing the mechanical properties of elastomers play interconnection matrix forming polymer chains or polymer network [15-31].

4.1.2 The distribution of transverse relaxation times T_2

Figure 4.2 shows normalized CPMG echo, on the first point, samples of reinforced EPDM with Ecorax® 1720 based on the content of fillers.

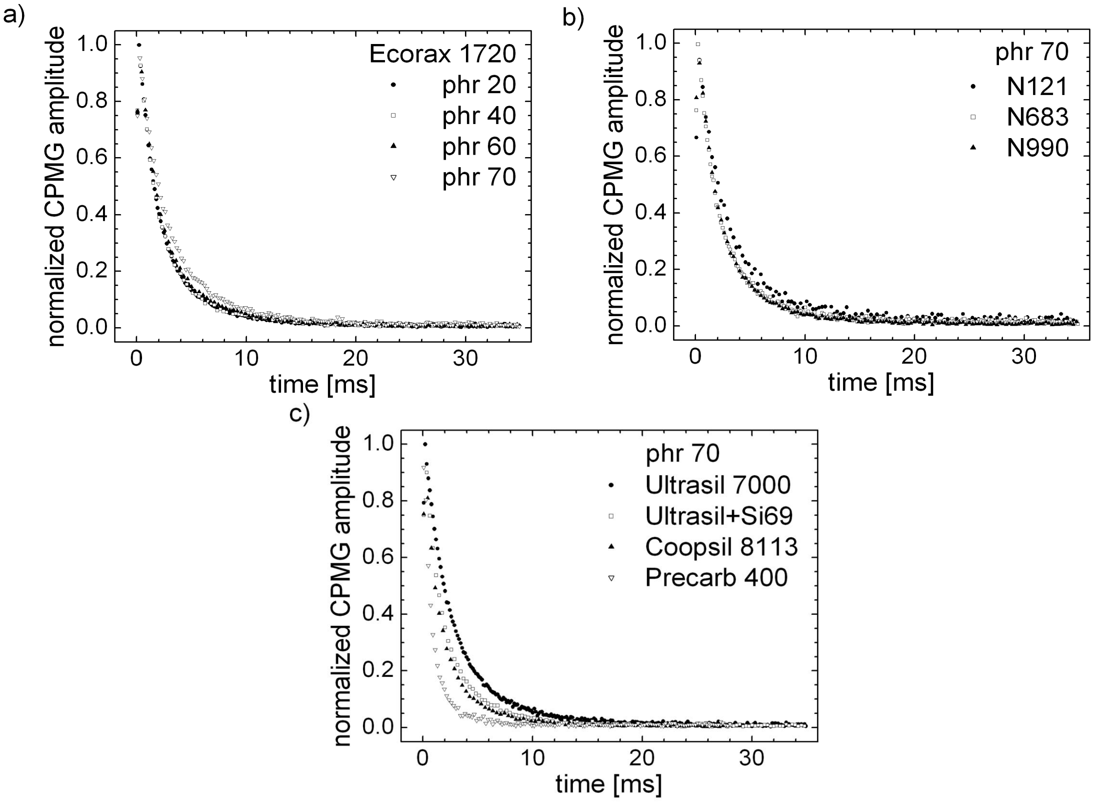

Fig. 4.2 Normalized CPMG decays of 500 echoes for a) the Ecorax filler samples versus filler concentration, and for the 70 phr filled sample versus b) carbon black N121, N683 and N990, and c) Ultrasil® 7000 GR, Ultrasil® 7000 GR +Si69, Coupsil® 8113 and Precarb® 400, filler types.

Tabel 4.1 Peaks center in T_2 distribution and relative peak integrals.

Sample	Filler content (phr)	Mixing energy [J/g]	$T_{2,\mathrm{short}}$ [ms]	A_{short} [%]	$T_{2,\mathrm{long}}$ [ms]	A_{long} [%]	$T_{2,\mathrm{out}}$ [ms]	A_{out} [%]
unfilled	0	1352	0.99	34.7	2.42	65.3	-	-
N121	20	1357	1.46	71.6	4.45	28.4	-	-
N121	40	1387	1.34	66.4	3.87	33.6	-	-
N121	60	1508	1.27	62.0	3.82	37.9	-	-
N121	70	1459	1.66	51.4	4.09	48.6	-	-
Ecorax® 1720	20	1338	1.37	68.0	4.02	32.0	-	-
Ecorax® 1720	40	1346	1.35	66.6	3.89	33.4	-	-
Ecorax® 1720	60	1442	1.53	70.2	4.48	29.8	-	-
Ecorax® 1720	70	1390	1.85	65.2	4.75	34.8	-	-
N683	20	1317	1.58	75.5	4.75	24.5	-	-
N683	40	1337	1.26	64.2	3.80	35.8	-	-
N683	60	1364	1.27	55.5	3.47	44.5	-	-
N683	70	1410	1.43	62.7	3.78	37.3	-	-
N990	20	1252	1.78	78.6	5.32	21.4	-	-
N990	40	1180	1.71	76.7	5.12	23.3	-	-
N990	60	1106	1.28	55.6	3.47	44.4	-	-
N990	70	1065	1.64	75.3	4.58	24.7	-	-
Ultrasil® 7000 GR	20	1330	1.50	72.6	4.62	18.5	0.34	8.9
Ultrasil® 7000 GR	40	1441	2.30	48.8	5.46	10.4	0.89	40.8
Ultrasil® 7000 GR	60	1346	1.24	63.5	3.63	36.5	-	-
Ultrasil® 7000 GR	70	1263	1.82	66.4	4.71	33.6	-	-
Ultrasil® 7000 GR + Si69	20	1291	1.28	68.2	4.02	20.8	0.28	11.0
Ultrasil® 7000 GR + Si69	40	1292	1.24	61.9	3.77	25.1	0.24	13.0
Ultrasil® 7000 GR + Si69	60	1329	1.34	69.9	3.85	30.1	-	-
Ultrasil® 7000 GR + Si69	70	1329	1.18	62.1	3.57	27.7	0.13	10.2
Coupsil® 8113	20	1403	1.46	72.1	4.50	27.9	-	-
Coupsil® 8113	40	1378	1.17	58.2	3.41	41.8	-	-
Coupsil® 8113	60	1435	1.45	62.5	4.09	25.5	0.57	12.0
Coupsil® 8113	70	1487	1.68	46.5	3.96	16.3	0.69	37.2
Precarb® 400	20	1181	1.43	66.4	4.47	17	0.25	16.6
Precarb® 400	40	1113	0.70	69.8	2.65	30.2	-	-
Precarb® 400	60	1059	0.35	71.4	1.42	28.6	-	-
Precarb® 400	70	1048	0.42	72.3	1.64	27.7	-	-

The fitting errors are smaller than 5 %

4.1.3 Filler effect of the T_2 distribution

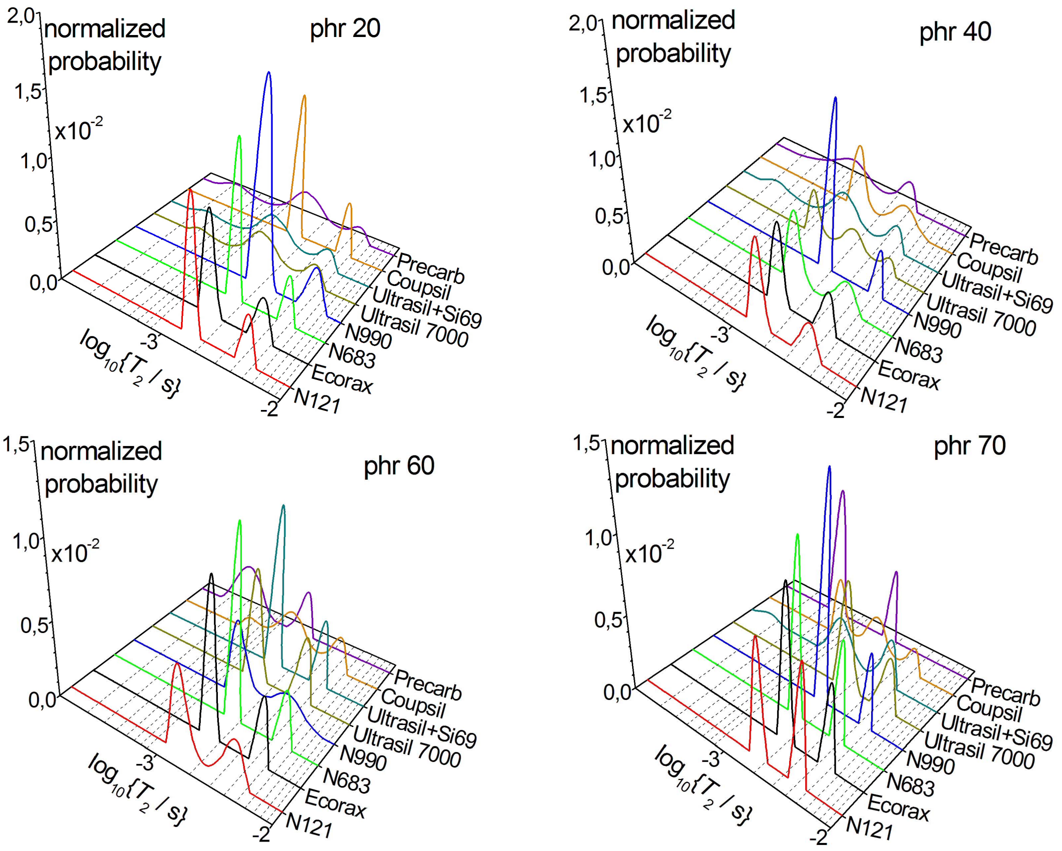

Fig. 4.4 Normalized distributions of transverse relaxation times with filler concentration a) 20 phr, b) 40 phr, c) 60 phr, and d) 70 phr for all filer of the series.

Figure 4.4 compares distributions of T_2 for the entire series of EPDM samples with filler concentration of 20 phr to 70 phr. The order of samples corresponds to that in Table 4.1, starting with carbon black fillers in order to increase particle size and surface area decrease.

A quantitative parameter to describe the effect of the filler polymer interaction is the

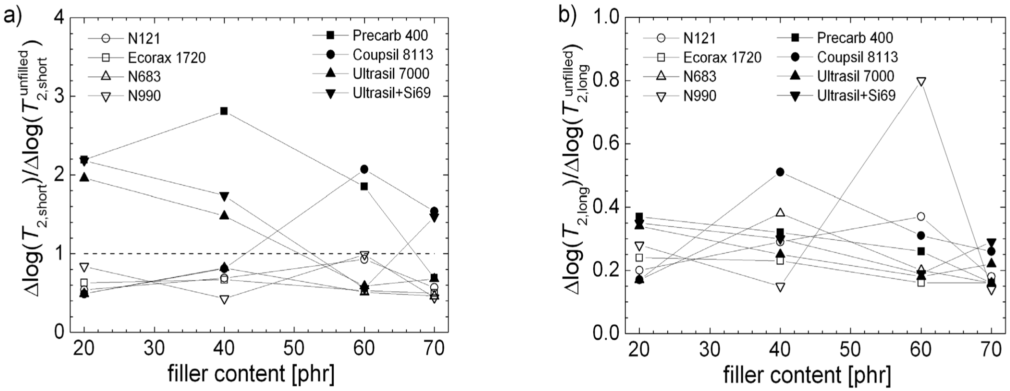

Fig. 4.5 Relative width at half height of the T_2 relaxation peaks for the a) short and b) long components for the entire series of filled EPDM samples. The continuous lines are drawn to guide the eyes. The horizontal dashed line in a) is drawn as a reference of normalization.

relative change $\Delta \log(T_2)/\Delta \log(T_2^{\text{unfilled}})$ in the width at half peak height extracted from the 1D distribution, which characterizes the T_2 distribution of the filled elastomers in relation to the one of the unfilled elastomers.

4.2.2 Interpreting of longitudinal relaxation times T_1 distributions for reinforced EPDM

The longitudinal relaxation distribution $f(T_1)$ is obtained in the same manner as $f(T_2)$ except for a change of the kernel function:

$$S_{\mathrm{T}_1}(\tau_1) = \int_0^{\infty} f(\mathrm{T}_1)\left\{1 - \exp\left(-\frac{\tau_1}{\mathrm{T}_1}\right)\right\} \mathrm{d}\,\mathrm{T}_1\,, \tag{4.3}$$

where, τ_1 is the relaxation period of time.

The recovery of longitudinal magnetization curve after saturation for the unfilled EPDM rubber is presented in Fig. 4.7a together with the associated distribution $f(T_1)$ of longitudinal relaxation times T_1 (Fig. 4.7b) according to Eq. (4.3). The low noise content of experimental data (open circles in Fig. 4.7a) ensures a good fit (continuous line in Fig. 4.7a) and provides confidence that the small peaks that appear in the T_1 distribution are real. The level of confidence in the validity of the low-intensity peaks observed in the measured T_1 distributions has been tested in form of the invariance of distribution with regard to changes of the distribution limits and/or number of points. The results confirm that the smallest peak observed in the T_1 distribution of the unfilled EPDM sample is real and not an artifact.

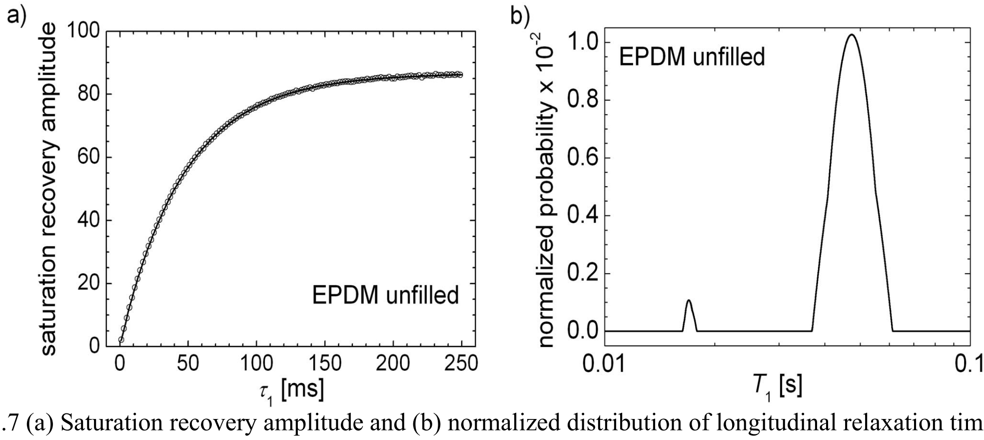

Fig. 4.7 (a) Saturation recovery amplitude and (b) normalized distribution of longitudinal relaxation times for the unfilled EPDM sample.

4.2.3 Fillers effect over T_1 distributions

Increase the amount of filler from 20 to 40 phr (Fig. 4.9) leads to grouping of signal in the T_1 distributions between 30 ms to 40 ms. Only Ecorax® 1720 leads to two clear peaks, where now more polymer segments small T_1 values than in the unfilled and 20 phr samples. Two more filler types, N121 and Ultrasil® 7000 GR, lead to an observable left shoulder in the T_1 peaks of mobile components. For the N683 filler this component is probably covered by the large line width and low height of a single peak. The other fillers lead to a single narrow peak in the T_1 distribution.

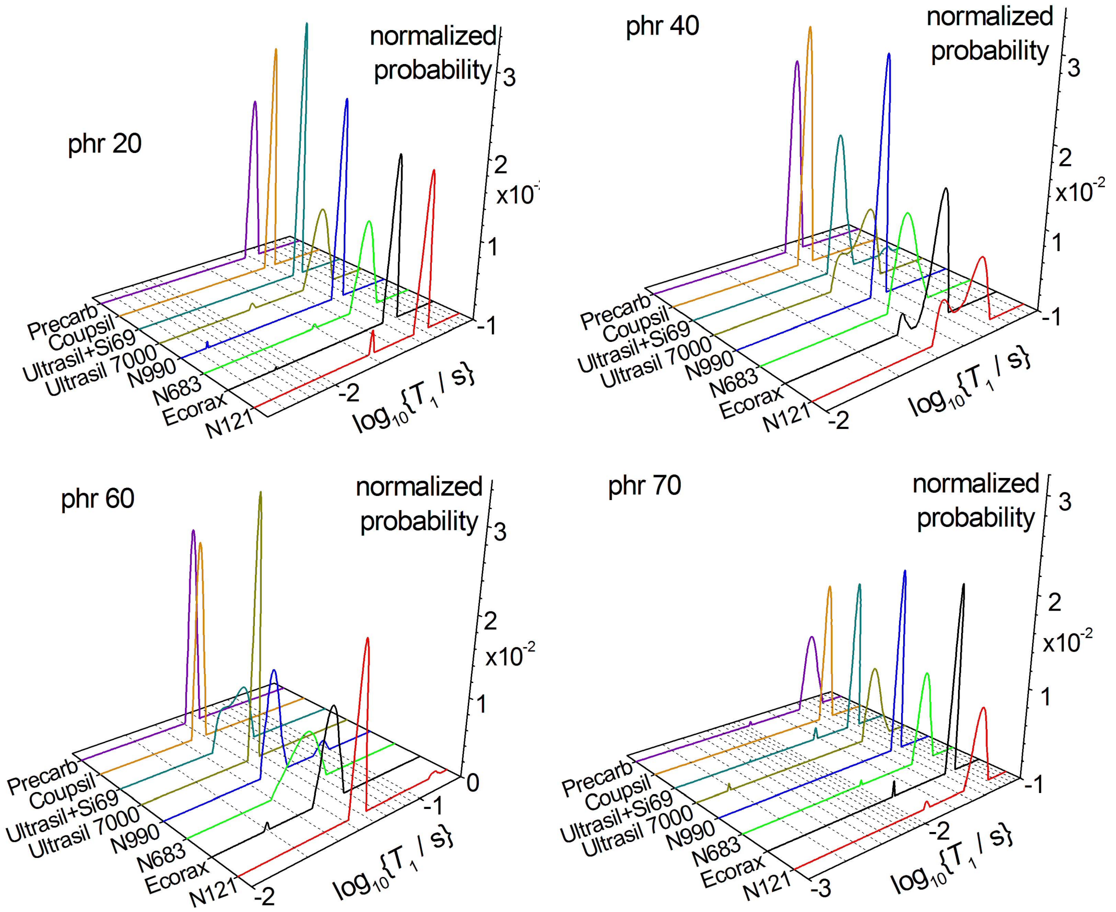

Fig. 4.9 Normalized distributions of longitudinal relaxation times T_1 for samples whit fillers concentration of (a) 20 phr, (b) 40 phr, (c) 60 phr, and (d) 70 phr for all fillers of the series.

4.3.3 Fillers effect over $T_{1\rho}$ distributions

The distribution function $f(T_{1\rho})$ of the longitudinal relaxation time $T_{1\rho}$ in rotating frame can be obtained in the same manner by Laplace inversion of experimental data as that for the T_2,

$$S_{T_{1\rho}}(\tau)=\int_0^\infty f(T_{1\rho})\exp\left(-\frac{\tau}{T_{1\rho}}\right)\mathrm{d}T_{1\rho}\ , \qquad (4.5)$$

where τ is the spin-lock pulse duration.

Generally, the $T_{1\rho}$ distributions can be interpreted in terms of two resolved of single wide peaks centered between 1 ms to 10 ms and a small peak at low $T_{1\rho}$ value, usually below 1 ms (Fig. 4.11). For small (20 phr Fig. 4.11a) and medium (60 phr Fig. 4.11c) filler content the peak at low $T_{1\rho}$ value represents only a small fraction of all polymer segments.

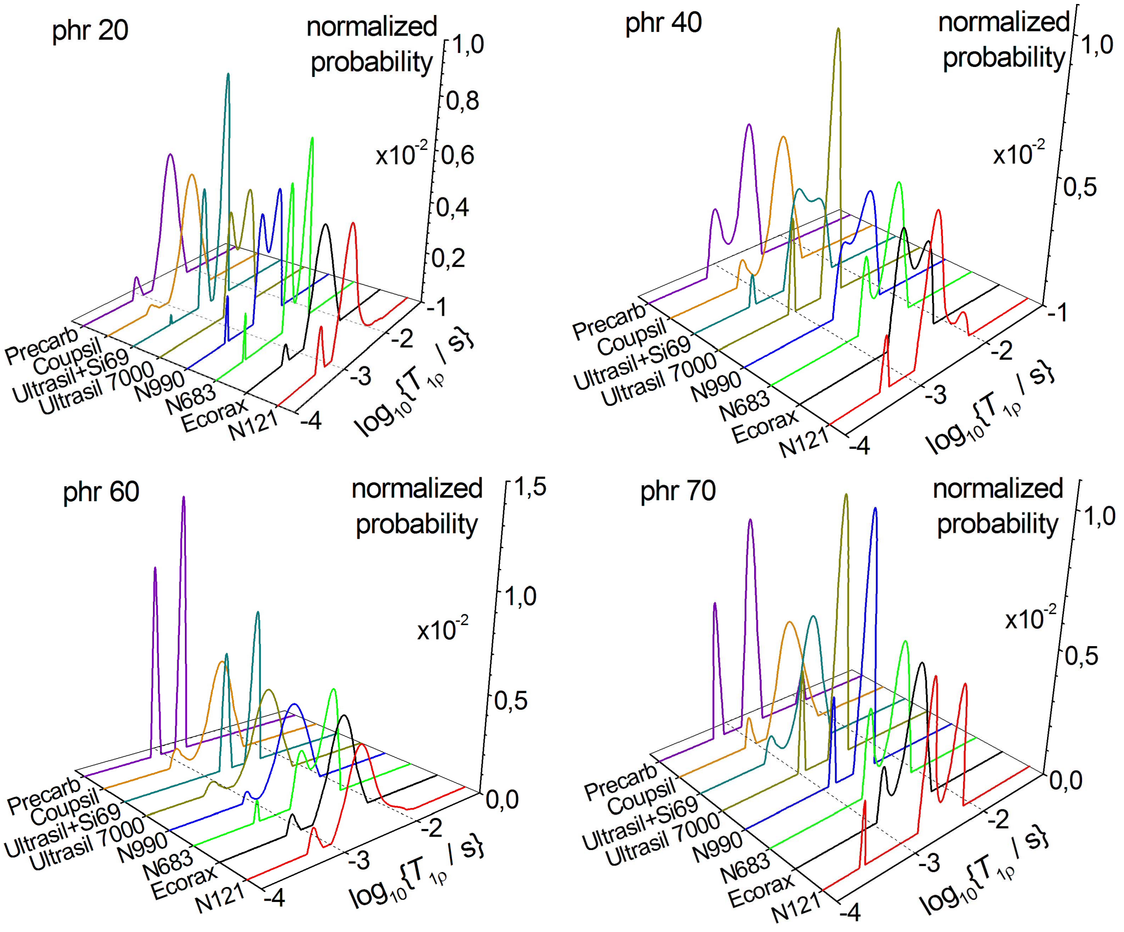

Fig. 4.11 Normalized distribution of longitudinal relaxation time $T_{1\rho}$ in rotating frame for the samples with filler concentrations of a) 20 phr, b) 40 phr, c) 60 phr, and d) 70 phr for the filler of the series.

Chapter 5. Heterogeneities of molecular dynamics shown by residual moments M$_2$ and correlation times τ_c

5.3 Hahn echo decay

The total spin Hamiltonian in the rotating frame which describes the free evolution of a dipolar coupled spin system is given by

$$\begin{aligned}\mathcal{H}(t) &= -\Delta\Omega\cdot \mathrm{I}_z + \overline{\mathcal{H}}_\mathrm{D} + \Delta\overline{\mathcal{H}}_\mathrm{D}(t)\\ &= -\Delta\Omega\cdot \mathrm{T}_{1,0} + \overline{\omega}_\mathrm{D}\mathrm{T}_{2,0} + \Delta\omega_\mathrm{D}(t)\mathrm{T}_{2,0}\end{aligned}, \tag{5.1}$$

where $\Delta\Omega$ is the off-resonance Hamiltonian [11, 13] and $\mathrm{T}_{1,0}$ is the irreducible tensor operator corresponding to the spin operator I_z, while the prefactors of the $\mathrm{T}_{2,0}$ irreducible tensor operator is related to the preaveraged dipolar interaction. $\Delta\overline{\mathcal{H}}_\mathrm{D}(t) = \mathcal{H}_\mathrm{D}(t) - \overline{\mathcal{H}}_\mathrm{D}$ is the part of the dipolar Hamiltonian fluctuating around the residual part given by [32-40].

The normalized decay of Hahn echo ^{1}H for $\Delta\Omega = 0$, may be write,

$$\frac{S_\mathrm{y}(2\tau)}{S_\mathrm{y}(0)} = \left\langle\cos(2\overline{\omega}_\mathrm{D}\tau)\right\rangle\left\langle\cos\left[\sqrt{\frac{3}{2}}\int_0^\tau \Delta\omega_\mathrm{D}(\tau')\mathrm{d}\tau' + \sqrt{\frac{3}{2}}\int_\tau^{2\tau}\Delta\omega_\mathrm{D}(\tau'')\mathrm{d}\tau''\right]\right\rangle. \tag{5.11}$$

where, the symbol $\langle(...)\rangle \equiv \left\langle\langle\ \rangle_{\vec{R}}\right\rangle_\beta$ represents the average over the statistical ensemble which includes two separate averages, one over the length of the reduced end-to-end vector $\vec{R}$, denoted by $\langle(...)\rangle_{\vec{R}}$ and the other over the azimuthally angle β denoted by $\langle(...)\rangle_\beta$.

$$\left\langle\cos[\phi(0,\tau)+\phi(\tau,2\tau)]\right\rangle = \exp\left\{-\left\langle\phi^2(0,\tau)\right\rangle\right\}\times\exp\left\{-\left\langle\phi(0,\tau)\phi(\tau,2\tau)\right\rangle\right\}. \tag{5.13}$$

In order to evaluate Eq. (5.13) we can introduce the dipolar correlation function [32, 35-36],

$$\int_0^t\int_0^t \left\langle\Delta\omega(t')\Delta\omega(t'')\right\rangle \mathrm{d}t'\,\mathrm{d}t'' = 2\int_0^t (t-t')C(t')\mathrm{d}t', \tag{5.14}$$

where a Gaussian distributed process of $\Delta\omega_\mathrm{D}(t)$ was assumed. The correlation function of the dipolar fluctuation, C(t) is considered to be of the exponential form [30, 32, 37] see down,

$$C(t) = \left\langle\Delta\omega_\mathrm{D}(t)\Delta\omega_\mathrm{D}(0)\right\rangle = \left\langle\Delta\omega_\mathrm{D}^2(0)\right\rangle\exp\{-t/\tau_\mathrm{c}\} = \widetilde{M}_2\exp\{-t/\tau_\mathrm{c}\}, \tag{5.15}$$

where the mean squared fluctuation of the dipolar coupling constant (5.15) is denoted by $\widetilde{M}_2 \equiv \left\langle\Delta\omega_\mathrm{D}^2(0)\right\rangle$, and τ_c is the correlation time of the segmental motions.

Considering Eq. (5.11), Eq. (5.13) and Eq. (5.15) the normalized Hahn-echo (HE) signal can be written as,

$$\frac{S_{\mathrm{HE}}(2\tau)}{S_{\mathrm{HE}}(0)} = \langle \cos(2\overline{\omega}_{\mathrm{D}}\tau) \rangle \left\langle \begin{array}{l} \exp\left[-2\sqrt{\frac{3}{2}}\widetilde{M}_2\tau_c^2\left(e^{-\tau/\tau_c} - 1 + \tau/\tau_c\right)\right] \\ \times \exp\left[-\sqrt{\frac{3}{2}}\widetilde{M}_2\tau_c^2\left(1 - 2e^{-\tau/\tau_c} + e^{-2\tau/\tau_c}\right)\right] \end{array} \right\rangle . \tag{5.16}$$

It is clear from Eq. (5.16) that the Hahn-echo signal for a spin-½ pair can be written as a product of averaged (av) and fluctuating (fl) contributions [33, 34] i.e.,

$$\frac{S_{\mathrm{HE}}(2\tau)}{S_{\mathrm{HE}}(0)} = \langle S_{\mathrm{av}}(\overline{\omega}_{\mathrm{D}}, \tau) \rangle \langle S_{\mathrm{fl}}(\Delta\omega_D, \tau_{\mathrm{c}}, \tau) \rangle , \tag{5.17}$$

where the average (or solid-like) contribution is given by,

$$S_{\mathrm{av}}(\overline{\omega}_{\mathrm{D}}, \tau) = \cos(2\overline{\omega}_{\mathrm{D}}\tau) , \tag{5.18a}$$

and the fluctuating (or liquid-like) contribution by,

$$S_{\mathrm{fl}}\left(\widetilde{M}_2, \tau_{\mathrm{c}}, \tau\right) = \exp\left[-\sqrt{\frac{3}{2}}\widetilde{M}_2\tau_c^2\left(e^{-2\tau/\tau_c} + 2\tau/\tau_c - 1\right)\right]. \tag{5.18b}$$

5.4 The contribution of polymer chains mobile segments at the Hahn echo decay

Three dynamical components of polymer chains in a filled elastomers can be considered as (see Fig. 5.3): i) the bound rubber ii) the interface between bound rubber and mobile chains; and iii) the mobile chains, with one end connected via interface to the bound rubber and the second end can be a free end or as in the majority of cases connected to another nano-cluster. One can consider that the bound polymer chains are characterized by strongly restricted motions compared to the interface and mobile chain segments. Both, the interface and mobile segments present a certain degree of freedom, therefore along this work will be consider unitary as mobile polymer segments, but with different dynamics. Then, the full NMR signal can be written as a sum of signals arising from the bound (bd) and mobile (mb) contributions,

$$\frac{S_{\mathrm{HEc}}(2\tau)}{S_{\mathrm{HEc}}(0)} = \left\langle S_{\mathrm{av}}^{\mathrm{bd}}\left(\overline{\omega}_{\mathrm{D}}^{\mathrm{bd}}, \tau\right)\right\rangle \left\langle S_{\mathrm{fl}}\left(\widetilde{M}_2^{\mathrm{bd}}, \tau_{\mathrm{c}}^{\mathrm{bd}}, \tau\right)\right\rangle + \left\langle S_{\mathrm{av}}^{\mathrm{mb}}\left(\overline{\omega}_{\mathrm{D}}^{\mathrm{mb}}, \tau\right)\right\rangle \left\langle S_{\mathrm{fl}}\left(\widetilde{M}_2^{\mathrm{mb}}, \tau_{\mathrm{c}}^{\mathrm{mb}}, \tau\right)\right\rangle , \tag{5.19}$$

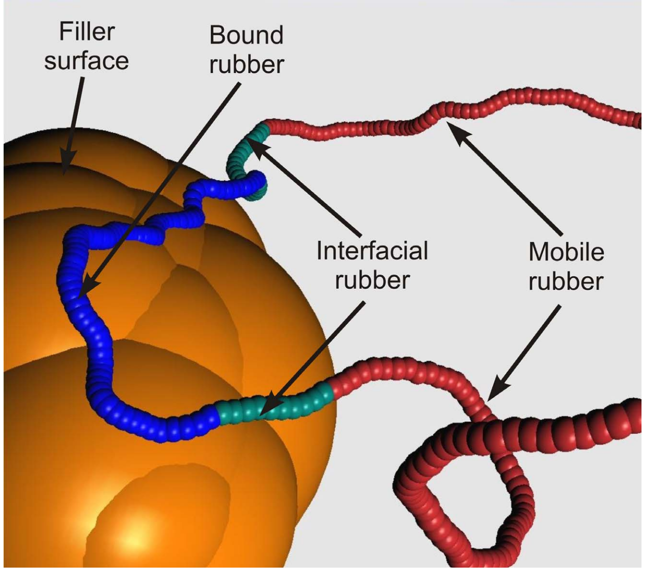

The schematic representation of interface between the EPDM chains rubber and clustered nano-particles fillers. The bond rubber characterized by a restricted chain dynamics is a consequence of strong direct interaction of fillers with polymer segments. This interaction will influence also the dynamics of intermediate chain segments.

In this approximation the final relationship that expresses the normalized Hahn-echo decay is in a good approximation described by,

$$\frac{S_{\mathrm{HEc}}(2\tau)}{S_{\mathrm{HEc}}(0)} = \left\langle S_{\mathrm{fl}}\left(\widetilde{M}_2^{\mathrm{mb}}, \tau_{\mathrm{c}}^{\mathrm{mb}}, \tau\right)\right\rangle = \left\langle \exp\left[-\sqrt{\frac{3}{2}}\widetilde{M}_2 \tau_c^2 \left(e^{-2\tau/\tau_c} + 2\tau/\tau_c - 1\right)\right]\right\rangle, \qquad (5.21)$$

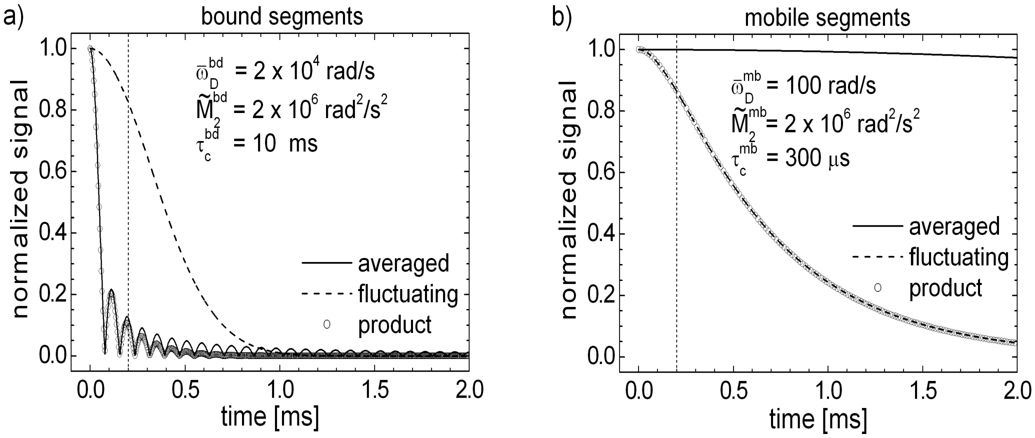

Fig. 5.4 Representation of normalized signals computed from Eqs. (5.18) for a) bound chain segments with $\overline{\omega}_{\mathrm{D}}^{\mathrm{bd}} = 2\times10^4$ rad/s, $\left\langle \widetilde{M}_2^{\mathrm{bd}} \right\rangle = 2\times10^6$ rad^2/s^2, $\tau_{\mathrm{c}}^{\mathrm{bd}} = 10$ ms and b) mobile chain segments with $\overline{\omega}_{\mathrm{D}}^{\mathrm{mb}} = 100$ rad/s, $\left\langle \widetilde{M}_2^{\mathrm{mb}} \right\rangle = 2\times10^6$ rad^2/s^2, $\tau_{\mathrm{c}}^{\mathrm{mb}} = 300\ \mu s$ averaged component (continues line – eq. 5.18a), fluctuating component (dash line – eq. 5.18b) and product (circles).

5.5 Evaluating of the medium residual moment M_2 of ^{1}H and correlation time

Table 5.1. Characteristics of unfilled and filled EPDM compounds averaged residual second moment, $\langle \widetilde{M}_2 \rangle$ the center of gravity, $\tau_{c,0}$ and width of decimal logarithm, $\Delta\tau_c$.

samples	Filler content (phr)	averaged values		distribution of correlation time		
		$\langle \widetilde{M}_2 \rangle$ (10^6 rad^2/s^2)	$\langle \tau_c \rangle$ (μs)	$\langle \widetilde{M}_2 \rangle$ (10^6 rad^2/s^2)	τ_{c0} (μs)	$\Delta\tau_c$
unfilled	0	2.45	230.5	1.76	341.4	0.24
N121	20	2.07	286.6	1.59	399.4	0.25
N121	40	2.72	238.4	2.05	335.2	0.47
N121	60	2.56	228.1	1.89	324.4	0.22
N121	70	2.20	294.6	1.95	340.6	0.14
Ecorax® 1720	20	2.18	261.3	1.71	349.9	0.21
Ecorax® 1720	40	2.42	259.4	1.93	340.8	0.20
Ecorax® 1720	60	3.17	189.5	3.18	288.8	0.21
Ecorax® 1720	70	2.26	273.2	1.97	321.7	0.14
N683	20	5.66	115.1	2.70	256.2	0.23
N683	40	3.44	181.5	2.25	294.6	0.23
N683	60	2.78	220.3	2.01	321.6	0.22
N683	70	2.19	280.7	1.76	369.2	0.21
N990	20	1.83	335.9	1.47	449.8	0.25
N990	40	2.55	244.5	1.95	337.9	0.21
N990	60	2.76	229.6	2.05	327.22	0.21
N990	70	2.60	237.7	2.00	324.9	0.20
Ultrasil® 7000 GR	20	1.89	342.2	1.62	419.56	0.193
Ultrasil® 7000 GR	40	2.13	271.1	1.90	309.46	0.130
Ultrasil® 7000 GR	60	4.26	142.6	2.67	235.3	0.176
Ultrasil® 7000 GR	70	3.67	163.3	2.63	234.1	0.153
Ultrasil® 7000 GR + Si69	20	2.84	214.3	1.98	327.7	0.237
Ultrasil® 7000 GR + Si69	40	5.29	111.0	2.59	236.7	0.205
Ultrasil® 7000 GR + Si69	60	2.78	234.4	2.06	336.8	0.219
Ultrasil® 7000 GR + Si69	70	2.31	261.5	1.87	338.5	0.189
Coupsil® 8113	20	28.52	21.44	2.95	216.7	0.223
Coupsil® 8113	40	31.62	21.11	3.86	180.8	0.213
Coupsil® 8113	60	30.55	20.39	2.30	287.8	0.211
Coupsil® 8113	70	29.82	19.88	2.30	270.8	0.20
Precarb® 400	20	30.29	20.2	2.56	249.9	0.19
Precarb® 400	40	52.04	20.3	4.03	409.6	0.599
Precarb® 400	60	51.28	20.3	25.73	61.72	0.482
Precarb® 400	70	47.24	20.5	19.66	70.20	0.472

5.7 Distribution of residual moment M_2 for ^{1}H

The fast Laplace inversion algorithm applied on the experimental data to determine the distribution of the residual second moment, $f\left(\widetilde{M}_2\right)$ has to consider now the Hahn-echo decay described by,

$$\mathrm{S}(\tau)=\sum_{i=1}^{N} f\left(\widetilde{M}_{2,\mathrm{i}}\right)\exp\left[-\sqrt{\frac{3}{2}}\widetilde{M}_{2,\mathrm{i}}\bar{\tau}_{\mathrm{c}}^{2}\left(\mathrm{e}^{-2\tau/\tau_{\mathrm{c}}}+2\tau/\bar{\tau}_{\mathrm{c}}-1\right)\right]\mathrm{d}\left[\log_{10}\left(\widetilde{M}_2\right)\right]. \tag{5.27}$$

The normalized distributions of ^{1}H residual second moments, $\widetilde{M}_2$ for the EPDM elastomers reinforced with carbon black fillers are presented in Fig. 7. The distributions were obtained by applying the inversion Laplace procedure using Eq. (5.27) where the average correlation time was taken to be $\bar{\tau}_{\mathrm{c}} = 312.3\,\mu s$. In order to be compared directly, all distributions are normalized; this means that the integer area under the distribution, in logarithmic scale, is unity (fig. 5.7).

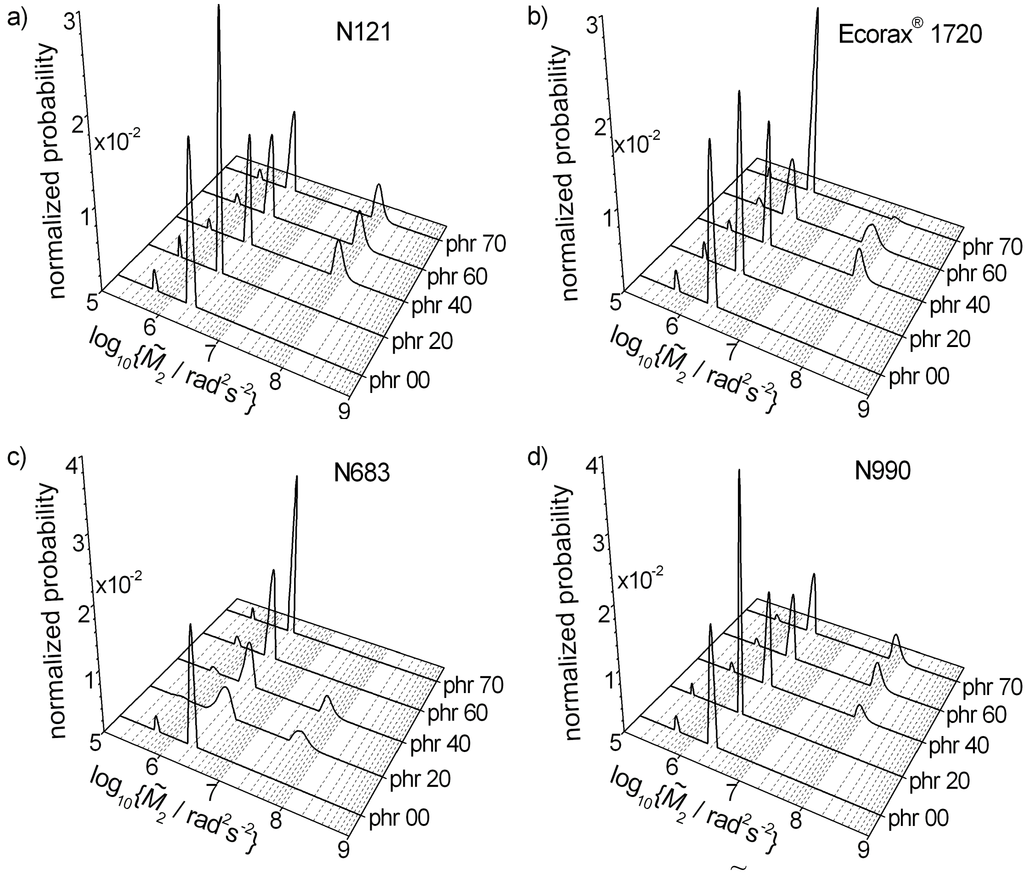

Fig. 5.7 Normalized probability distribution of residual second moment, $\widetilde{M}_2$ for the EPDM samples filed with the series of carbon black fillers (a) N121, (b) Ecorax®1720, (c) N683, and (d) N990 for 20, 40, 60 and 70 phr filler contents. The normalized probability distribution for unfilled EPDM is also shown.

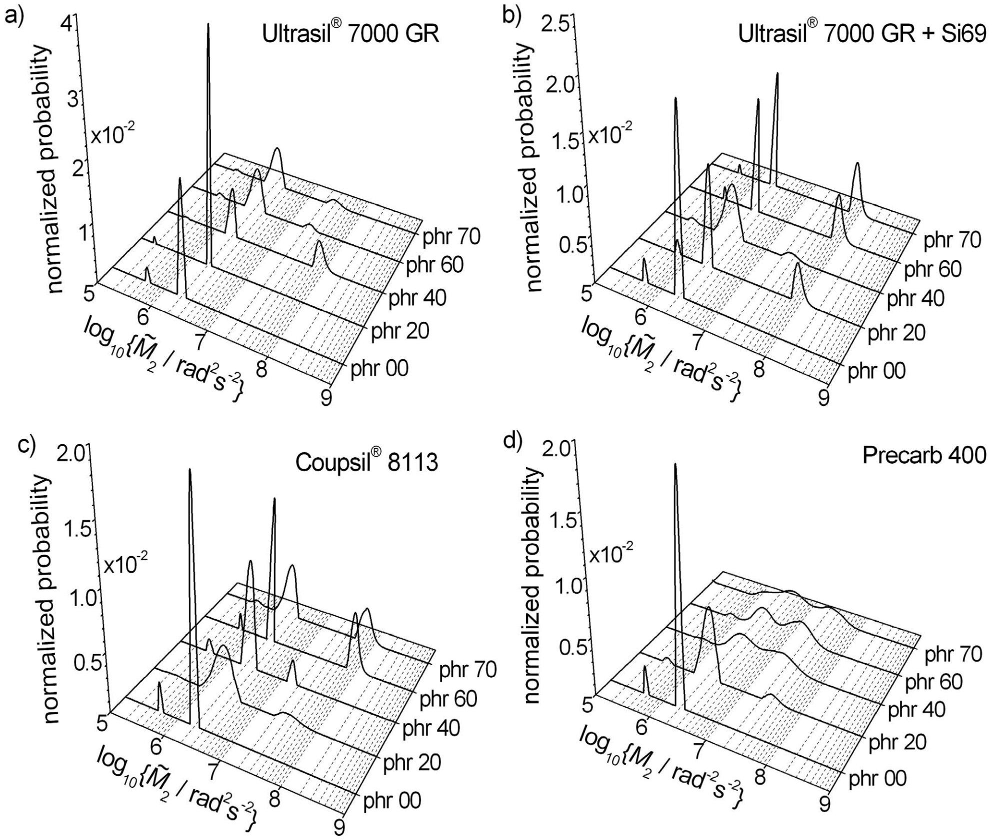

Fig. 5.8 Normalized probability distribution of residual second moment, $\widetilde{M}_2$ for EPDM samples filed with the series of non-carbon black fillers: (a) Ultrasil® 7000 GR, (b) Ultrasil® 7000 GR+Si69, (c) Coupsil® 8113, and (d) Precarb® 400 for 20, 40, 60 and 70 phr filler contents. The normalized probability distribution for unfilled EPDM is also shown.

The effect of filler content on the EPDM polymer segments is more pronounced for the non-carbon black filler as can been shown in Fig. 5.8. The distribution of residual second moment for the samples reinforced with Ultrasil® 7000 GR at 20 phr filler content is characterized by two peak (Fig. 5.8a). For this sample, the $f(\widetilde{M}_2)$ distribution consists of one narrow peak and a second smaller peak observed at one order of magnitude lower than the main peak. For medium and large filler contents the apparition of the interface polymer chains characterized by peaks with one order of magnitude higher of $\widetilde{M}_2$ values is evidenced. We can conclude that this large effects on the residual second moment distributions of samples with Precarb® 400 must not been identified with a strong filler – polymer chain interaction but with a more heterogeneous interaction originated from the diversity of filler aggregate/agglomerate topology.

Chapter 6. NMR experiments of multi quants used in elastomers characterization

6.1.2 Highlighting of aging effects in two quanta curves

The effect of aging in the normal condition after one year can be observed by the apparition of a new component in the double quantum build up curves, like a shoulder shifted on bigger values by comparison with the maxim of non-aging sample (see fig 6.2 unfilled circles).

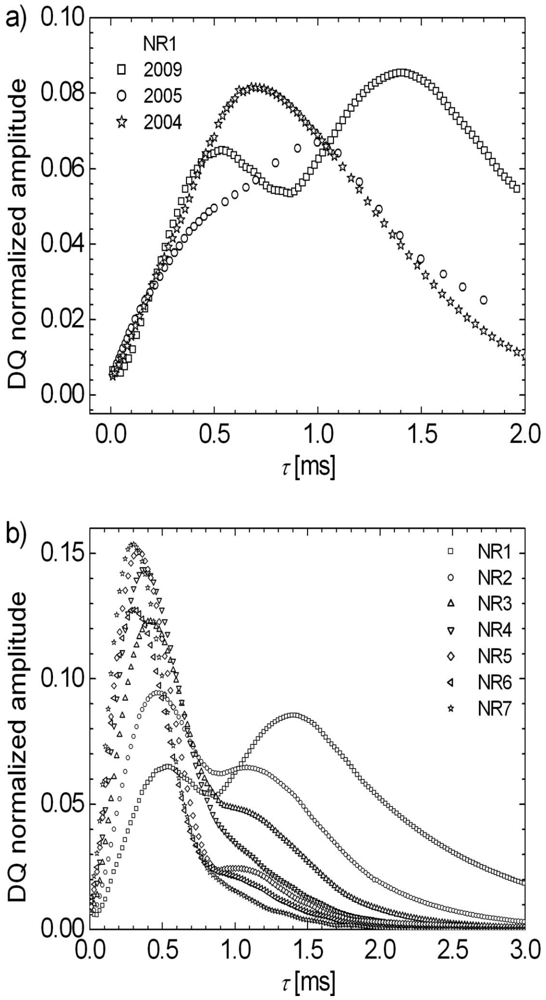

Fig. 6.2 Duble quantum build up curves for cross-link natural rubber aging in natural condition a)measured in time, after one year (2004), two years (2005) and six years (2009); and b) measured after six years after fabrication data in function of cross-link density for NR1-NR7.

6.1.4 Fourier spectrum in approximately of spin pears -½

For a spin - ½ pair all the terms of the Hamiltonian described by Eq. (6.1) commute with each other which allows obtaining an exact evaluation of the spin system response.

$$S_{DQ}(2\tau)=\left\langle \sin^2(\overline{\omega}_\mathrm{D}\tau)\exp\left(-\frac{2\tau}{T_2}\right)\right\rangle, \tag{6.5}$$

$$\begin{aligned}\mathcal{FT}\left\{S_\mathrm{DQ}(2\tau),T_2^*\right\}&=\mathcal{FT}\left\{-\left\langle \sin^2(\overline{\omega}_\mathrm{D}\tau)\exp\left(-\frac{2\tau}{T_2}\right)\right\rangle+\frac{1}{2}\exp\left(-\frac{2\tau}{T_2^*}\right)\right\}\\ &\cong\frac{1}{2}\mathcal{FT}\left\{\left\langle \cos(2\overline{\omega}_\mathrm{D}\tau)\exp\left(-\frac{2\tau}{T_2}\right)\right\rangle\right\}\end{aligned}, \tag{6.8}$$

where T_2^* is effective correlation of the transverse relaxation time.

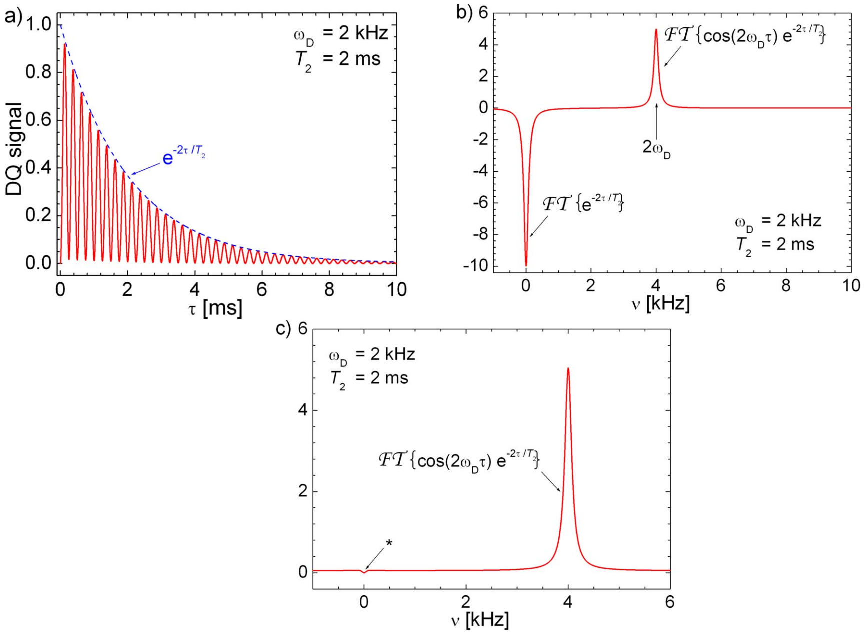

Fig. 6.4 2 a) Signal of DQ coherences simulated by an exponential function and transversal relaxation time was fixed at 2 ms for $\omega_D = 2kHz$; b) Fourier transform, c) corected Fourier spectrum.

6.1.6 Fourier spectrum in approximately of isolated CH$_2$ and CH$_3$ groups

$$\begin{aligned}\mathcal{FT}\left\{S_\mathrm{DQ}(2\tau)\right\}&=\mathcal{FT}\left\{\begin{matrix}-\frac{4}{7}\left\langle \sin^2\left(\overline{\omega}_D^{(CH_2)}\tau\right)\exp\left(-\frac{2\tau}{T_2^{(CH_2)}}\right)\right\rangle-\frac{9}{35}\left\langle \sin^2\left(\overline{\omega}_D^{(CH_3)}\tau\right)\exp\left(-\frac{2\tau}{T_2^{(CH_3)}}\right)\right\rangle\\ +\frac{29}{70}\exp\left(-\frac{2\tau}{T_2^*}\right)\end{matrix}\right\}\\ &\cong\frac{1}{14}\mathcal{FT}\left\{\left\langle 4\cos\left(2\overline{\omega}_D^{(CH_2)}\tau\right)\exp\left(-\frac{2\tau}{T_2^{(CH_2)}}\right)\right\rangle+\left\langle \frac{9}{5}\cos\left(2\overline{\omega}_D^{(CH_3)}\tau\right)\exp\left(-\frac{2\tau}{T_2^{(CH_3)}}\right)\right\rangle\right\}\end{aligned}. \tag{6.12}$$

6.1.8 Two quanta Fourier spectrum characterization

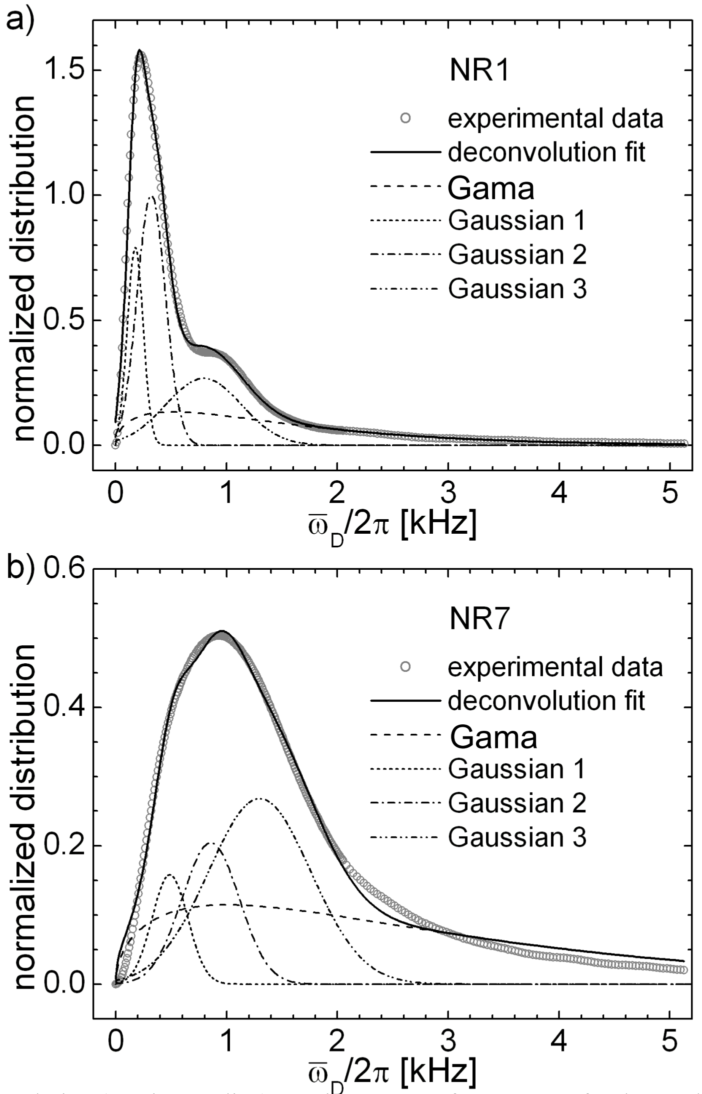

Fig. 6.8 Fitting deconvolution (continuous line) Fourier spectra of two quanta for the aged samples a) NR1 and b) NR7 described by eq. (6.19).

Fourier spectrum of two quantum of natural rubber cross-link aged consists of two components. Fourier fitting for these spectra with a sum of Gaussian functions for each of Γ and two components lead to inconclusive results. Instead, the best fitting (continuous line) was found when two quanta Fourier spectrum (open circles) was solved with a function Γ (dotted line) and three Gaussian functions (represented by small dotted line, dash-dot-line and line-dot-dot). Results presented in Figure 6.8 for NR1 and NR7 old.

6.2 Characterization of the reinforced EPDM heterogeneities by DQ measurements

6.2.1 DQ curves depending on the type and filler concentration

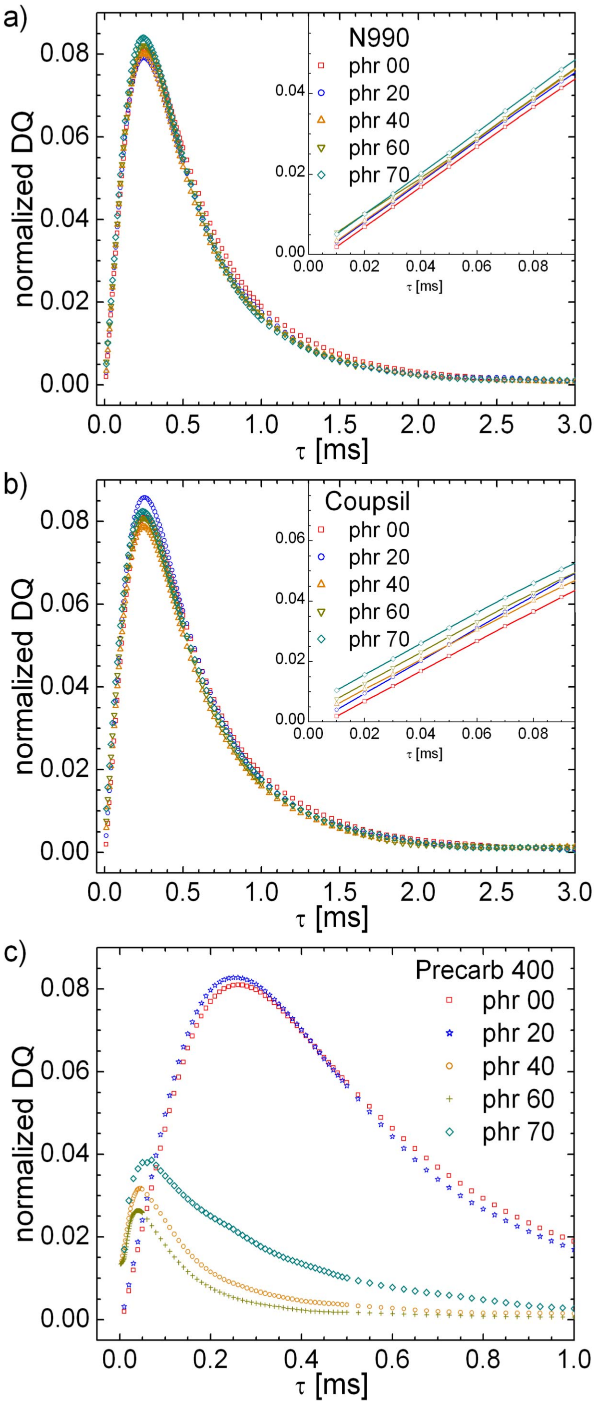

Fig. 6.10 The DQ build-up curve represented function of excitation/reconversion time τ up to 3 ms for a series of EPDM samples unfilled and filled with 20, 40, 60 and 70 phr filler content of a) N990; b) Ultrasil 700 GR and c) Precarb 400. In order to see the fine differences between samples, the same DQ build-up curves are represented in the medallions of figure a) and b) for the excitation/reconversion time τ up to 0.1 ms..

6.2.2 Effects of filer-polymer interactions over the polymeric chain dynamics

Graphical representation of the residual dipole coupling constant depending on the filler content from 20 to 70 phr reinforced EPDM samples with different fillers are shown in Figure 6.13. Thus in Figure 6.13 is observed carbon black filler type N121 blue square, red circles Ecorax 1720, orange triangles pointing up N683 and N990 upside down triangles. The clear dependence of the residual dipole coupling constant depending on the filler content is observed in samples N990 and Ecorax 1720, in contrast to the other two samples at concentrations of 70 PHR can see a slight decrease in dependence.

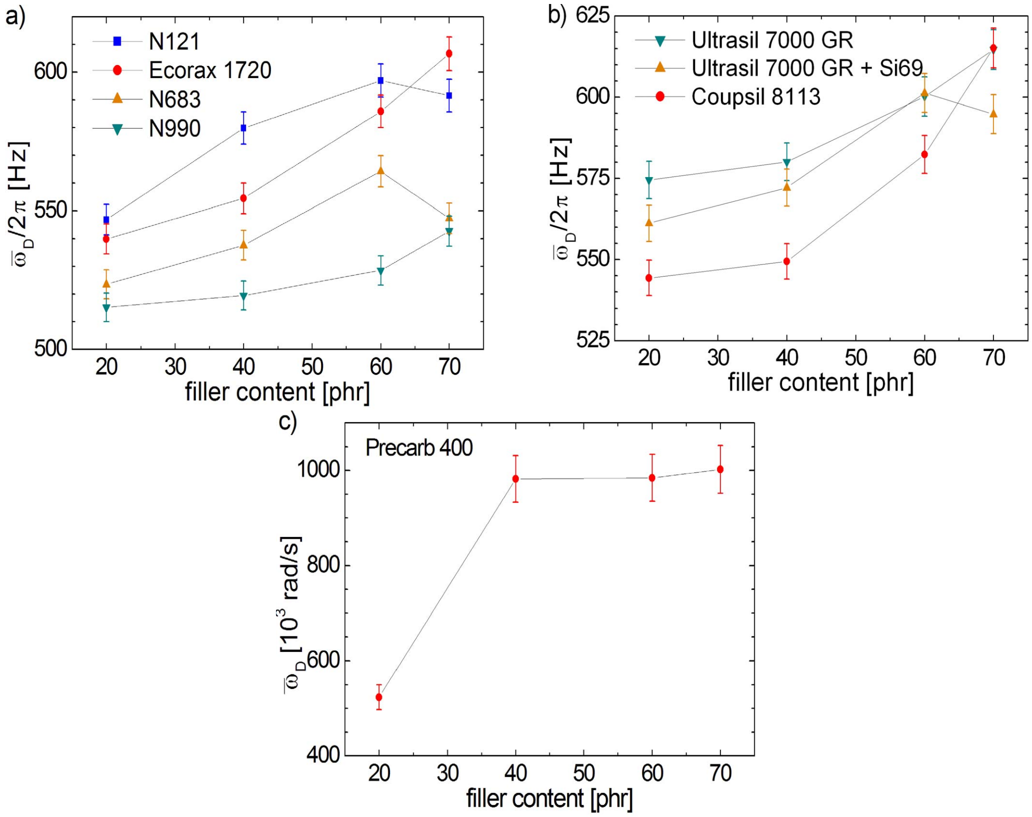

Fig. 6.13 The plots of residual dipolar coupling constant function of filler contents from 20 to 70 phr for the EPDM samples filled with a) carbon black fillers: N121 (blue square), Ecorax 1720 (red circle), N683 (orange up-triangle) and N990 (dark cyan down-triangle); b) silica based: Ultrasil 700 GR (dark cyan down-triangle), Ultrasil 700 GR +Si 69 (orange up-triangle) and Coupsil 8113 (red circle) and c) Precarb 400. The thin lines are drawn to guide the eye.

Chapter 7. Morphology of the nanocomposit polymers and biopolymers shown by spin diffusion measurements

Overlap between the Abragamian peaks and Lorentzian peaks type. Magnetization of segments connected is the dominating segments related to the time of diffusion of small spins, this is even more evident at higher filler content (see Figure 7.5b). After diffusion of spin magnetization was found in most of the mobile segments. Contrary to expectations the "Abragam" character is not observed during the lowest diffusion of t_d = 164.8 μs [41-48].

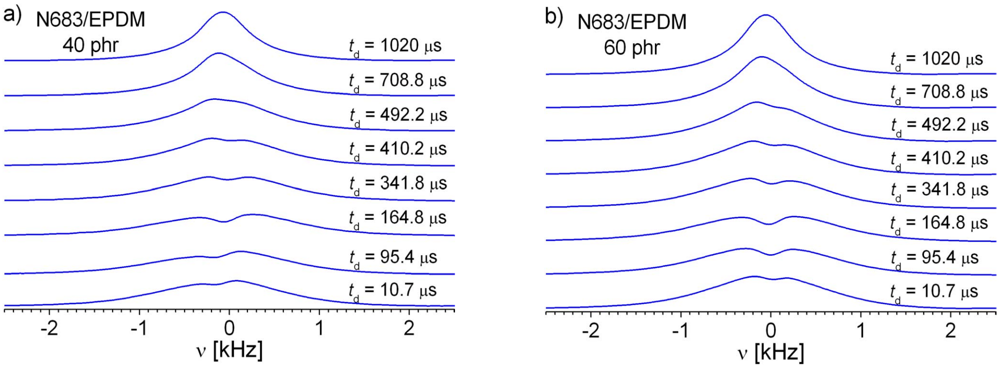

Fig. 7.5 The DQ filtered Fourier spectra, superposition of Abragamian and Lorentzian functions, for the EPDM samples filled with a) 40 phr and b) 60 phr N683 filler content for some particular values of spin diffusion time t_d = 10.7 μs, 95.4 μs, 164.8 μs, 341.8 μs, 410.2 μs, 492.2 μs, 708.8 μs, and 1020 μs.

7.2 Spin diffusion for reinforced EPDM samples

Experimental distributions for bigger diffusion time t_d than 490 μs.

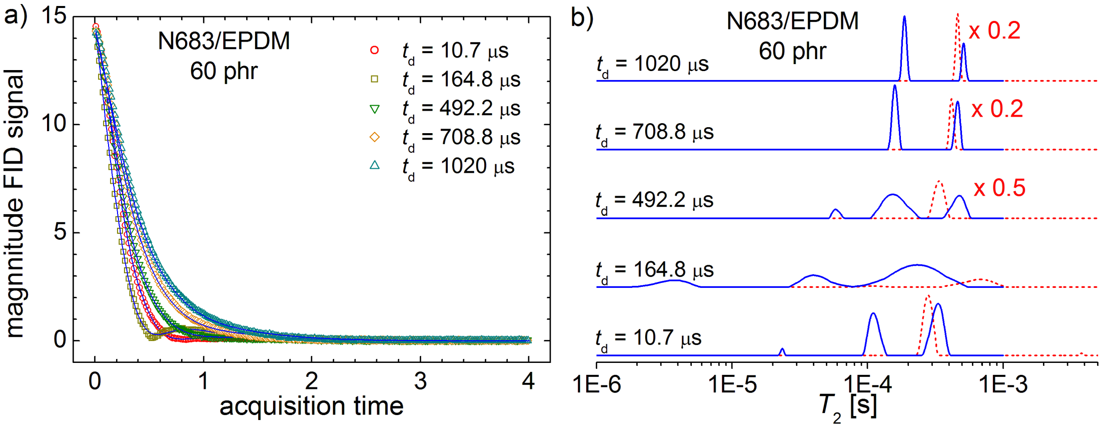

Fig. 7.6 a) The magnitude FID decays for EPDM samples filled 60 phr N683 filler content for some particular values of spin diffusion time t_d = 10.7 μs (circle), 164.8 μs (square), 492.2 μs (down-triangle), 708.8 μs (rhomb), and 1020 μs (down-triangle), and the corresponding fits (line). b) The Abragamian (continuous line) and exponential (dashed line) distributions of transverse relaxation time T_2, obtained by bi-kernel Laplace inversion of experimental FID decays shown in Fig. a) for the same sample and the same spin diffusion times. The exponential peaks at a t_d larger than 490 μs were multiplied with appropriate factor to be well fitted in scale.

7.3 Marginal chain morphology and dynamics in hydrated α keratin fibers

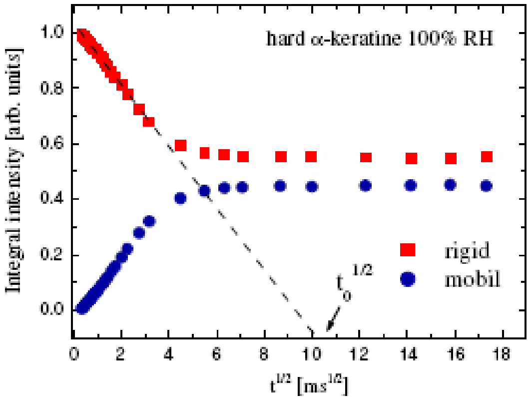

Fig. 7.11 Decay and buildup spin-diffusion curves from normalized integral spectral intensity. The straight line describing initial-rate behavior intersects the horizontal axis at $\sqrt{t_0}$ [41-48].

Whole areas of rigid and mobile components of the ^{1}H NMR spectrum measured at different times of spin diffusion are shown in fig. 7.11 for α keratin hydrated 100%

$$\frac{\bar{d}_R}{\bar{d}_R^{dry}} = \sqrt{\frac{\Delta\nu_{1/2}t_0}{\Delta\nu_{1/2}^{dry}t_0^{dry}}}\sum_{n=1}^{\infty}S_n \Big/ \sum_{n=1}^{\infty}S_n^{dry} \qquad (7.16)$$

Figure 7.12 is shown the size dependence of the average relative rigid areas for dry α keratin strongly in function of relative humidity, where you can see that magnetization transfer of mobile water in the initial region of spin diffusion is not essential.

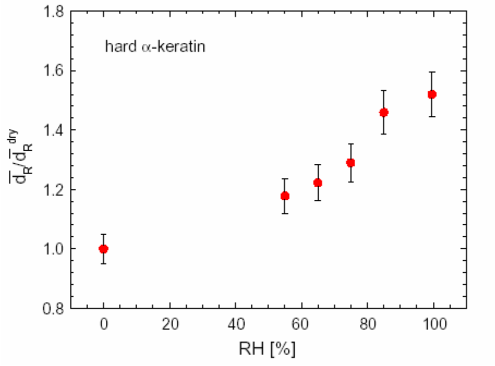

Fig. 7.12 The dependence of the relative average size of rigid domains for hard α keratin as a function of relative humidity [41].

Chapter 8. Modern NMR methods highlighting exchange processes

8.2 Describing and interpreting of the 2D T_2-T_2 correlation maps

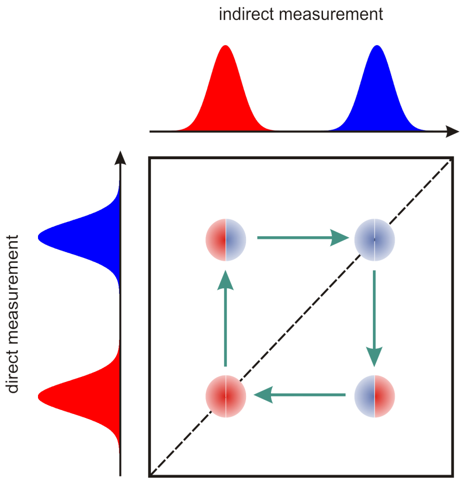

Fig. 8.2 Simulated CPMG pulse sequence (left) and the corresponding T_2 distributions (right), obtained by Laplace inversion, in the presence of molecular exchange as function of exchange time from a) $T_{2,1}$ = 400 ms to $T_{2,2}$ = 40 ms; b) uniformly between 10 ms and 50 ms; c) given by Maxwell-Boltzmann function as function of maximum of distribution, t_0; d) Maxwell-Boltzmann distribution function with t_0 = 20 ms for $T_{2,1}$ = 4 ms to 40 ms and $T_{2,2}$ = 40 ms to 4 ms.

8.3 Ultra-fast molecular exchange processes

Chemical exchange describes the migration of chemical groups from one chemical site to other site. If these sites are described by different relaxation rates then the new tool of analysis is 2D relaxation exchange NMR, where the initial and final states are encoded at two successive times with an exchange time between. The resulting 2D NMR spectra are anticipated to be interpretable in terms of diagonal peaks that represent the molecular population from sites in which the properties remain unchanged and off-diagonal peaks that indicate the molecular exchange. The 2D ^{1}H NMR exchange spectra were recorded using the T_2–M_Z(store)–T_2 pulse sequence with a period of magnetization storage between the two T_2 relaxation encoding periods.

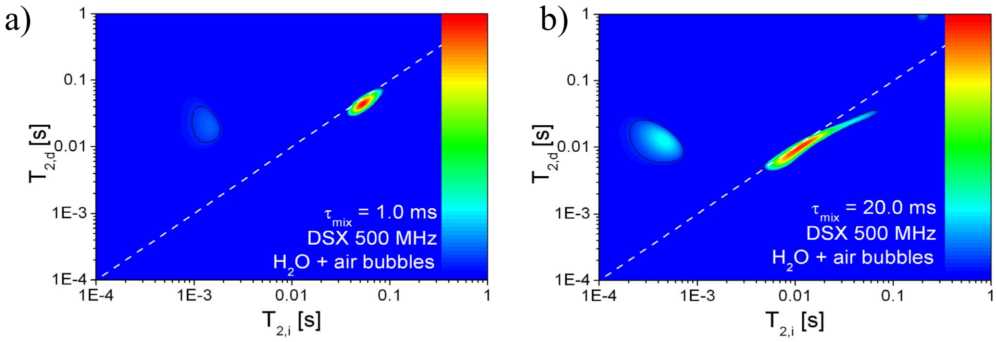

Fig. 8.4 2D ^{1}H NMR T_2-T_2 exchange maps of air bubbles in water recorded with mixing (exchange) times of τ_{mix} = 1 ms (a) and τ_{mix} = 20 ms (b).

8.4 Monte-Carlo simulation

8.4.2 Interpretation of the T_2-T_2 correlation maps in molecular exchange presence

The effects of molecular exchange processes on the two-dimensional (2D) NMR T_2-T_2 distributions obtained by Laplace inversion were studied by numerical simulations. The Monte–Carlo technique is used to generate free random walks of a large number of molecules within space regions characterized by different relaxation times. Molecular exchange processes are considered during CPMG encoding periods as well as during the exchange time. Systematic simulations were performed as function of NMR parameters like the exchange time and geometric or physical system properties.

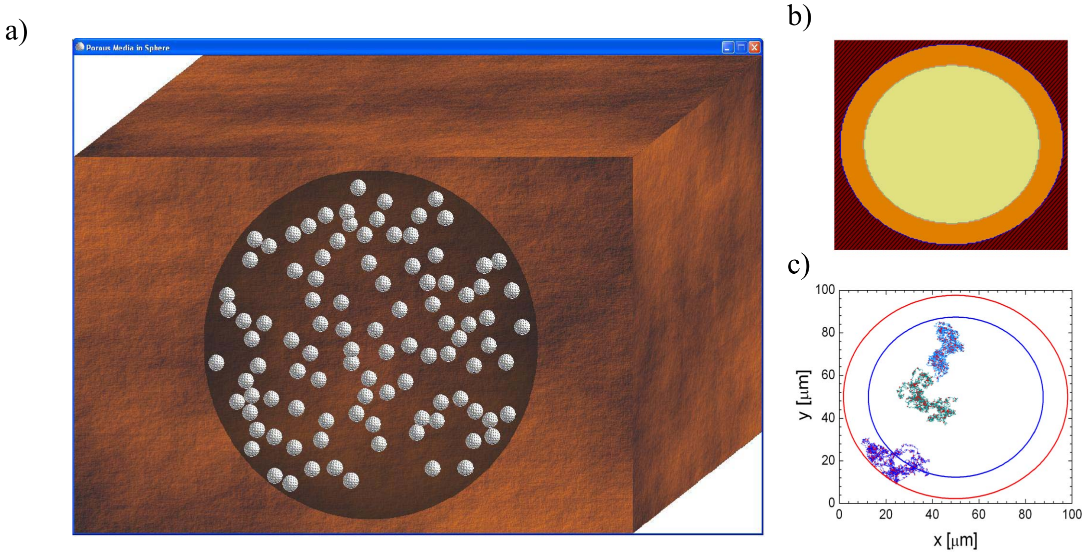

Fig. 8.5 Porous material with ideal spherical pore free molecule containing to move freely in all three directions, b) two-dimensional map of the relaxation times for which the material represented by hatching vertical; c) Monte Carlo simulation of movement of liquid molecules with random steps, free in the pore.

8.4.3 T_1 longitudinal relaxation time effect

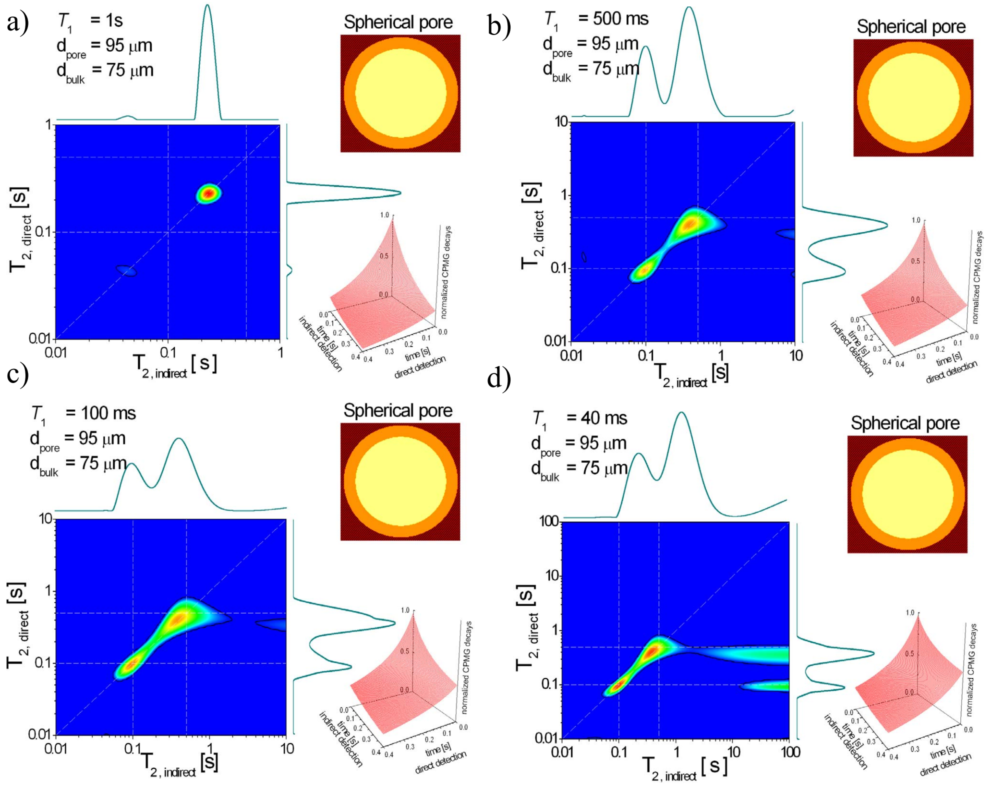

Fig. 8.8 Simulated 2D T_2–T_2 exchange maps for spherical pores in function of T_1 a) T_1= 1 s; b) T_1= 0.5 s; c) T_1= 0.1s and d) T_1= 0.04 s; D = 2.299 x 10^{-9} [m^2/s] and store time τ_{store} = 20 ms.

8.4.4 The effect of geometry, connectivity and size of the pores

The molecular dynamics and the particular geometry of system can lead to a single off-diagonal peak (Fig. 8.9). Such a single cross-peak it is often observed in the experimental data for fast exchange rates. The simulation of 2D T_2–T_2 exchange maps of two spherical pores with the same diameter d_{pore} connected directly through a channel of length $d_{channel}$ presents this prevalent exchange. For a suitable distance between two pores,

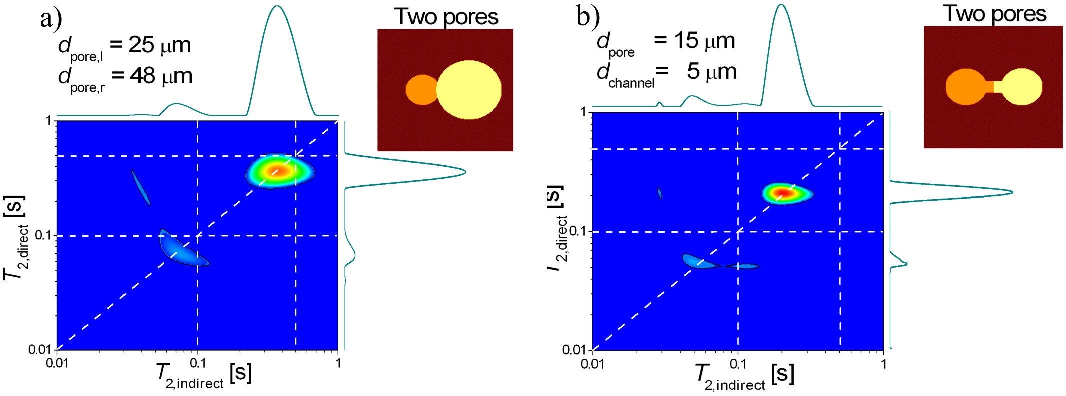

Fig 8.9 Simulated 2D T_2–T_2 exchange maps at τ_{store} = 20 ms and D = 2.299 × 10^{-9} m^2/s for two pores connected a) directly; b) via a channel.

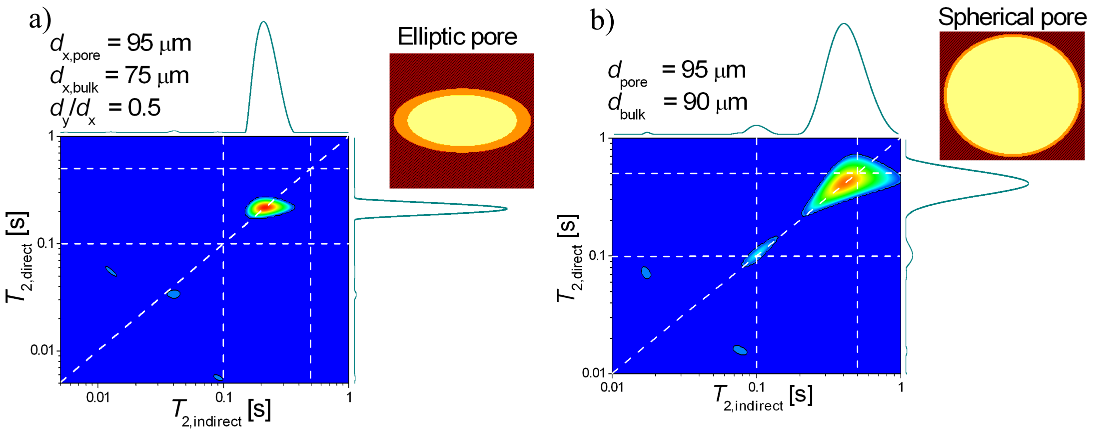

Fig. 8.10 Simulated 2D T_2–T_2 exchange maps at τ_{store} = 20 ms and D = 2.299 × 10^{-9} m^2/s for two pores connected a) elliptically pore; b) large pore with a small shell of surface water.

the classical pattern with two diagonal and two off-diagonal peaks is obtained (Fig. 2b). Geometrical factors of the system can be taken into account by changing the pore shape (Fig. 8.10). In Fig. 8.10 the thickness of the pore shell, which is often described in terms of the surface–to–volume ratio, can have a great influence on the appearance of 2D T_2–T_2 exchange maps.

8.5.1 Bi-dimensional T_2-T_2 exchange maps for the natural rubber

For the first time presents two-dimensional NMR measurements of T_2–T_2

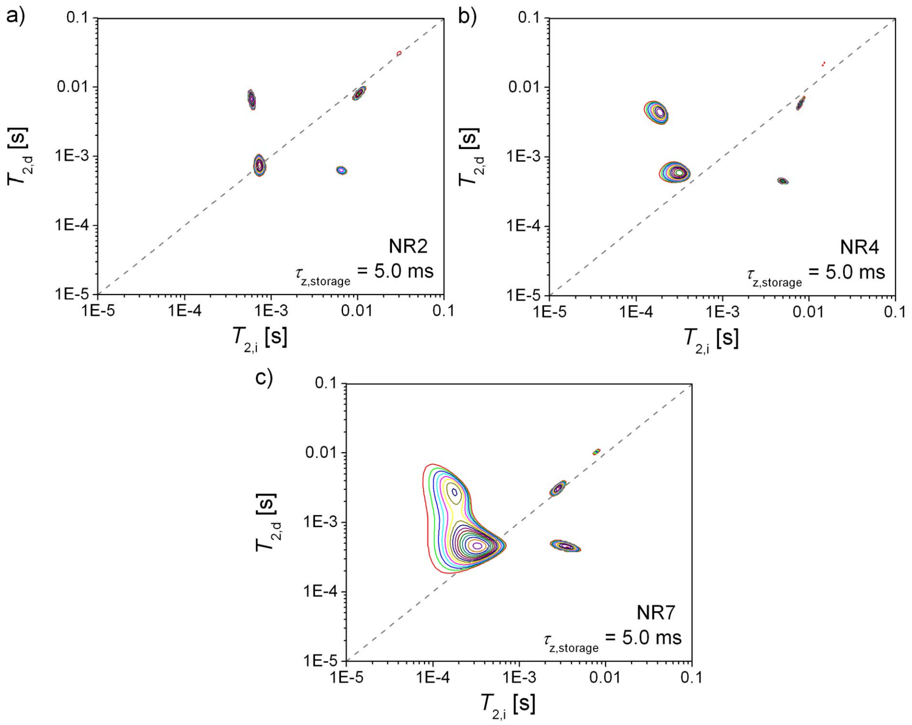

Fig. 8.12 2D T_2-T_2 exchange process NMR for a) NR2, b) NR4, c) NR7, $\tau_{z,storage}$ = 5 ms.

magnetization exchange with a storage period of magnetization between two periods T_2 coding for semi-solid samples.

8.5.2 Exchange time determination

Fitting parameters for samples NR1, NR4 and NR7 are presented in Table 8.1. Note that decreases with increasing exchange during cross-link density. Whole areas of peak-sized extra-diagonal left and bottom right corner of T_2-T_2 maps recorded according NR4 sample storage times are represented in Figure 8.14.

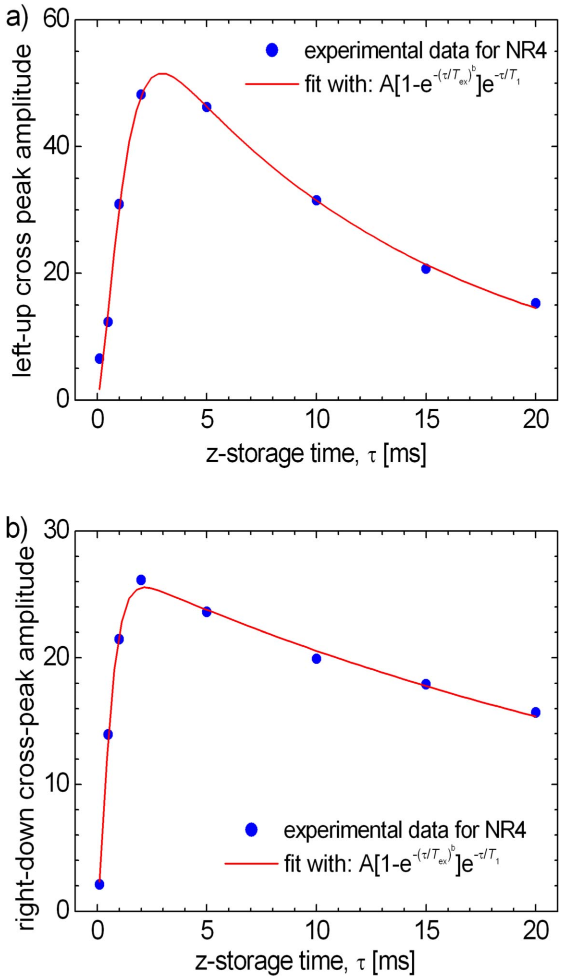

Fig. 8.14 2D representation of NMR exchange maps T_2-T_2 (2D) registered for NR4.

Table 8.1 Exchange time, T_{ex} and T_1 for cross-peaks left-up and right-down for T_2–T_2 exchange maps for NR1, NR4 and NR7.

Samples	left-up				Right-down		
	T_{ex}^{LU-CP} [ms]	T_1^{LU-CP} [ms]	b		T_{ex}^{RD-CP}	T_1^{RD-CP}	b
NR1	4.0	23.6	1		5.3	17.9	1
NR4	1.4	12.9	1.4		0.7	34.0	1.3
NR7	0.7	23.5	1.8		0.7	16.9	1.8

8.5.3 Bi-dimensional T_2-T_2 exchange maps specific to the filler EPDM

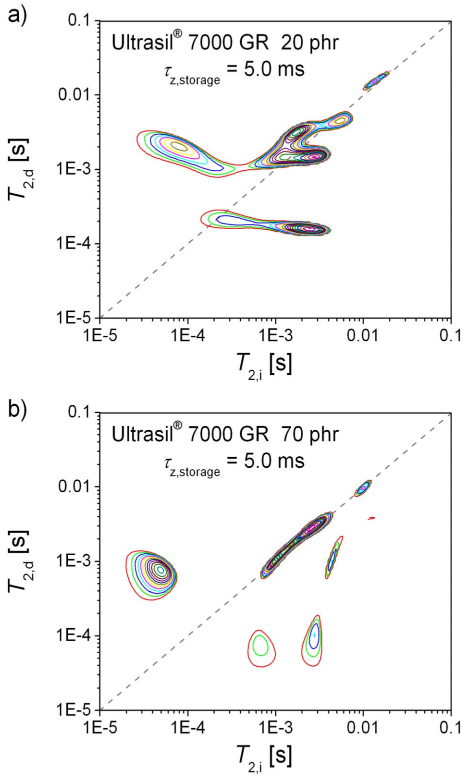

Fig. 8.15 2D representation of NMR exchange maps T_2-T_2 (2D) registered for the same sample Ultrasil 7000 with $\tau_{z,storge}$ = 5 ms,.

Chapter 9. Conclusion selections

This thesis presents new NMR applied methods into studying Nano-composite materials such as EPDM elastomers with filers, vulcanized natural rubber and α keratin. These methods combine experimental and theoretical NMR technics with Laplace transform based signal analyze and also with numerical simulations, especially Monte Carlo. So, for a series of reinforced EPDM samples with different types of fillers and in different concentrations the torsion module G' was measured, depending on the torsion amplitude, γ_0. It was shown that the storage module increases with the increase of the filler content regardless the filler type. For this kind of materials, with viscoelastic properties, the logarithmic representation of the torsion module regarding the torsion amplitude shows the high degree of heterogeneity of the filler-filler interaction distributions which assume to be responsible for the so called Payne effect. So, for low filler content, from linear dependences (in logarithmic scale) of G' regarding γ_0 there could be shown two types of interactions: i) filler-filler direct interactions and ii) indirect filler-filler interactions mediated by the polymer matrix

The dynamic heterogeneities of the polymer chains which mediate filler-filler interactions were studied in detail with specific NMR relaxometry methods. From the relaxation times distribution it was shown that the heterogeneity degree, which can be associated with the complexity of the interactions type and which modifies the polymer chain segments dynamics in the presence of fillers, increases with the increase of the filler content. Distributions for more specific parameters such as transverse relaxation times T_2, longitudinal T_1 and longitudinal in the system $T_{1\rho}$, as $\widetilde{M}_2$ residual moments and correlation times τ_c, were obtained by applying the reverse Laplace transform, uni-dimensional over the measured experimental curves.

Combined analysis of the distribution of the relaxing times and of the bi-dimensional distributions T_1–T_2 leads to the identification of more components of dynamic nature corresponding to the polymeric chain segments which result from the complex interactions of the polymer matrix with filler clusters.

The first effect, observed even at a low of 20 phr fillers, it is little movement in the distribution of T_2 at higher values. This indicates an increase in mobility of polymer chain segments. Another effect is the appearance of second peak narrow distributions of T_2 which suggests the presence of a highly dynamic local inhomogeneity polymer chain segments.

The third effect of Nano-fillers in the addition of the EPDM polymer matrix of T_2 distributions observed in the study is to increase the percentage amount of polymer chains characterized by low levels of T_2. They indicate the increasing number of segments of polymer chains that chain polymer-filler interaction due will have limited movement so less mobile.

The addition of fillers to the EPDM polymer matrix can lead to an increase in the amount of less mobile components for non-carbon black fillers and a decrease in bandwidth distribution compared with the values obtained for samples with no fillers or carbon-type fillers black. Dynamic heterogeneity corresponding segments exclusively mobile polymer chains were studied in the corresponding proton Hahn echo loss, measured with the acquisition delay that plays dipole filter that eliminates the signal contribution coming from the polymer chain segments related to the agglomeration of fillers. Thus Hahn echo drops measured are sensitive only to the polymer chain fluctuating mobile segments.

A systematic study of the dynamics heterogeneity of polymer chains for a series of EPDM elastomers with different filler types and contents, from 20 phr to 70 phr, was presented. The measurements used ^{1}H Hahn-echo decays for which the acquisition delay plays the role of a dipolar filter and will filtered out the signal arising from the bound polymer chains. The Hahn-echo decay weighted only by the fluctuating part of the mobile polymer chains was evaluated theoretically. It was showed that the decay depends in the first approximation on the average values of $\left\langle \overline{M}_2 \right\rangle$ and $\left\langle \tau_c \right\rangle$. These quantities were measured for a series of EPDM sample with different fillers and filler content. For carbon black fillers the values of $\left\langle \overline{M}_2 \right\rangle$ and $\left\langle \tau_c \right\rangle$ will increase with the filler content showing a reduction in the segmental motions due to the presence of filler aggregates and agglomerates. For instance, the N990 carbon-black filler has the size larger than that of N121 and the former filler exhipeaks also the smallest surface area (Table 1). These filler characteristics could be correlated with the larger values of $\left\langle \overline{M}_2 \right\rangle$ and $\left\langle \tau_c \right\rangle$ (Table 2). Such behaviour is also evident for Precarb® 400 but is less evident for silane fillers.

Increase curves of two quanta for a series of natural rubber cross-link natural aging have been characterized for the first time by interpreting the Fourier spectrum. For this interpretation a numerical program was written in C++ that lead to a correction with an effective relaxation time. Thus corrected Fourier spectrum revealed the specific features of distribution of residual dipole couplings. By comparison with other methods we can conclude that two quantum Fourier spectrum can be treated in terms of overlapping Gaussian distributor of couplings and residual Γ dipole.

Measurements were made by spin diffusion filter based on a dipole on EPDM samples for the entire series of fillers. For the first time applied to inverse transform Lapalce was used, the kernel is complex composed by two function one Abragamian and one exponential. Other spin diffusion measurements allowed characterization of keratin-α morphology. Decrease curves of spin diffusion have been interpreted theoretically in a cylindrical morphology. To calculate the relative size of the fields rigid depending on the degree of hydration i) writing a program in C++ that allowed the sum of 10^6 values of the roots of functions Bessel specific and ii) was fitted the initial part of experiments curves with a right to cross-axis radical diffusion time value $t_{0.}$

We have developed two-dimensional Laplace spectroscopy to characterize molecular exchange processes and magnetization exchange. These processes are highlighted by i) the appearance of little cross-peaks sites and ii) changes little diagonal sites of the 2D correlation maps of T_2-T_2. Amplitude area full-sized peak extra depending on the time diagonal storage of nuclear magnetization along the magnetic field was calculated theoretically. Unlike the theoretical calculations of amplitudes and positions slightly off-diagonal sites observed in 2D correlation maps of T_2-T_2 experimental high-speed exchange processes are not symmetrical. For the particular features of T_2-T_2 maps correlation experimental simulation program written in C++ for modeling MONTE-CARLO water exchange processes in porous media.

Monte-Carlo folders based on a reading of relaxation times has been very wavering the study of effects of self-diffusion coefficient value, the ratio between longitudinal relaxation time affecting NMR signal during storage magnetization along the field during this static magnetic storage, pore size, pore geometry and connectivity of their position on the amplitude and peak-sized diagonal and off-diagonal correlation of 2D maps of T_2-T_2.

For the first time have revealed the exchange magnetization processes for soft solid materials such as vulcanized natural rubber and EPDM elastomers with fillers type of 2D correlation maps based on T_2-T_2 two-dimensional inverse Laplace transform.

Selective Bibliography

[1] T. A. Vilgis, G. Heinrich, M. Klüppel, Reinforcement of polymer nano-composites, Theory, Experiments and Applications, Cambridge University Press, 2009

[2] Shinzo Kohjiya, Atushi Katoh, Toshiya Suda, Junichi Shimanuki, Yuko Ikeda, Visualisation of carbon black networks in rubbery matrix by skeletonisation of 3D-TEM image, Polymer, 47, 3298–3301 (2006).

[3] K. Gorna, M. Hund, M. Vucak, F. Grohn, G. Wegner, Amorphous calcium carbonate in form of spherical nanosized particles and its application as fillers for polymers, Materials Science and Engineering A, 477, 217–225 (2008).

[4] V. Herrmann, K. Unseld, H.-B. Fuchs, B. Blümich, Colloid Polym. Sci., 280, p. 758 (2002).

[5] P. J. McDonald, Prog. Nucl. Magn. Reson. Spect. 30, 69-99 (1997) and references therein.

[6] M.-J. Wang, Rubber Chem. Technol., 71, 520 (1998).

[7] D. Moldovan, R. Fechete, D. E. Demco, E. Culea, B. Blümich, V. Herrmann, M. Heinz, Heterogeneity of Nanofilled EPDM Elastomers Investigated by Inverse Laplace Transform ^{1}H NMR Relaxometry and Rheometry, Macromol. Chem. Phys., 211, 1579-1594 (2010).

[8] G. J. Kraus, Appl. Polym. Sci. Appl. Polym. Symp. 39, 75 (1984).

[9] A.-J. Zhu, S. S. Sternstein, Compos. Sci. Technol., 63, 1113 (2003).

[10] R. L. Klinberg, A. Sezginer, D. D. Griffin, M. Fukuhara, J. Magn. Reson., 97, 466 (1992).

[11] G. Eidmann, R. Savelsberg, P. Blümler, B. Blümich, J. Magn. Reson. A, 122, 104 (1992).

[12] Q. W. Yuanb, J. E. Mark, Macromol. Chem. Phys., 200, 206 (1999).

[13] D. Moldovan, R. Fechete, D. E. Demco, E. Culea, B. Blümich, V. Herrmann, M. Heinz, The heterogeneity of segmental dynamics of filled EPDM by ^{1}H transverse relaxation NMR, J. Magn. Reson., 208 156-162 (2011).

[14] J. Leblanc, *Prog. Polym. Sci.* 2002, *27*, 627.

[15] V.J. McBrierty, J.C. Kenny, *Kautsch. Gummi Kunstst.* 1994, 47, 342.

[16] V. M. Litvinov, P. A, M. Steeman, *Macromolecules* 1999, *32,* 8476.

[17] R. A. Orza, Pieter C. M. M. Magusin, Victor M. Litvinov, Martin van Duin, and M. A. J. Michels, *Macromolecules* 2007, *40,* 8999.

[18] V. Herrmann, K. Unseld, H.-B. Fuchs, B. Blümich, *Colloid Polym. Sci.* 280, 2002, p. 758.

[19] P. J. McDonald, Prog. Nucl. Magn. Reson. Spect. 30, 69-99 (1997) and references therein.

[20] Z. Zhu, T. Thompson, S. Q Wang, E. D. von Meerwall, A. Halasa, *Macromolecules* 2005, *38,* 8816.

[21] M.-J. Wang, *Rubber Chem. Technol.* 1998, *71*, 520.

[22] G. *J.* Kraus, *Appl. Polym. Sci.: Appl. Polym. Symp.* 1984, *39*, 75.

[23] T. A. Vilgis, Polymer, 2005, 12, 4223.

[24] G. Heinrich, M. Klüppel, T.A. Vilgis, Reinforcement theories in Physical Properties of Polymers Handbook 2nd Edition, Springer, Heidelberg, 2007

[25] Sternstein, S. S.; Zhu, A.-J. *Macromolecules* 2002, *35*, 7262.

[26] A.R. Payne, J. Appl. Polym. Sci. 1962, 6, 57.

[27] A.Roychoudhury, P. P. De, J. App. Polym. Sci. 1995, 55, 9.

[28] R. L. Klinberg, A. Sezginer, D. D. Griffin, M. Fukuhara, J. Magn. Reson. 1992, 97, 466.

[29] R. Kimmich, NMR: Tomography, Diffusiometry, Relaxometry, Springer-Verlag, Berlin, Heidelberg, New York, (1997).

[30] G. J. Bowden si W.D. Hutchinson, Tensor operator formalism for multiple-quantum NMR 1. Spin-1 nuclei, J.Magn. Rezon, 67,403-414, (1986).

[31] G. J. Bowden si W.D. Hutchinson, Tensor operator formalism for multiple-quantum NMR 2. Spin-3/2, 2 and 5/2 and General I, J.Magn. Rezon, 67,415-437, (1986).

[32] R. C. Ball, P. T. Callaghan, E. T. Samulski, A Simplified Approach to the Interpretation of Nuclear Spin Correlations in Entangled Polymeric Liquids, J. Chem. Phys., 106, 17, (1997).

[33] P. T. Callaghan and E. T. Samulski, The Molecular Weight Dependence of Nuclear Spin Correlations in Entangled Polymeric Liquids, Macromolecules, 31 3693-3705 (1998).

[34] P. T. Callaghan and E. T. Samulski, Molecular Ordering and the Direct Measurement of Weak Proton-Proton Dipolar Interactions in a Rubber Network, Macromolecules**,** 30, 113-122 (1997).

[35] D. A. Vega, M. A. Villar, and E. M. Vallés, C. A. Steren and G. A. Monti, Comparison of Mean-Field Theory and ^{1}H NMR Transversal Relaxation of Poly(dimethylsiloxane) Networks, Macromolecules, 34, 283-288 (2001).

[36] J.-P. Cohen-Addad, NMR and Fractal Properties of Polymeric Liquids and Gels, In Progress in NMR Spectroscopy; Emsley, J. W., Feeney, J., Sutcliffe, L. H., Eds.; Pergamon Press: Oxford, 25, 1-316 (1993).

[37] P. Sotta, C. Fülber, D. E. Demco, B. Blümich, and H. W. Spiess, Effect of Residual Dipolar Interactions on the NMR Relaxation in Cross-Linked Elastomers, Macromolecules, 29 6222-6230 (1996).

[38] Claudiu Melian, Dan E. Demco, Monica Istrate, Andreea Balaceanu, D. Moldovan, Radu Fechete, Crisan Popescu, Martin Möller, Morphology and side-chain dynamics in hydrated hard a-keratin fibres by ^{1}H solid-state NMR Chemical Physics Letters 480 (2009) 300–304.

[39] Maria Baias, Dan E. Demco, Daniel Istrate, Crisan Popescu, Bernhard Blümich, and Martin Moller, Morphology and Molecular Mobility of Fibrous Hard α-Keratins by ^{1}H, ^{13}C, and ^{129}Xe NMR, J. Phys. Chem. B 2009, 113, 12136–12147.

[40] J. Wang, on the determination of domain sizes in polimers by spin diffusion, J. Chem. Phys.,(1996) 104(12), 4850-4858.

[41] A. Abragam, *The principles of Nuclear Magnetism*, Clarendon Press Oxford, prima editie 1961, reprint 1996.

[42] L. Venkataramanan, Y. Q. Song, M. D. Hürlimann, *Solving Fredholm Integrals of the first kind with tensor product structure, IEEE Trans. Sig. Process*, 50, 1017-1026, 2002.

[43] Y. Q. Song, L. Venkataramanan, M. D. Hürlimann, M. Flaum, P. Frulla, and C. Straley, *T_1-T_2 correlation spectra obtained using a fast two-dimensional Laplace inversion*, J. Magn. Reson. 154, 261-268, 2002.

[44] M. D. Hürlimann, M. Flaum, L. Venkataramanan, C. Flaum, R. Freedman, G. J. Hirasaki, *Diffusion-relaxation distribution functions of sedimentary rocks in different saturation states*, Magn. Reson. Imag. 21, 305 – 310, 2003.

[45] T. Yokomizo, M. Nakasako, T. Yamazaki, H. Shindo, J. Higo, Chem. Phys. Lett. 401 (2005) 332.

[46] R. Fechete, D. Moldovan, D. E. Demco, and B. Blümich Laplace Inversions Applied to Multi–Component T_2–T_2 Exchange Experiments, Diffusion Fundamentals 10 (2009) 14.1 - 14.3.

[47] D. Moldovan, R. Fechete, D. E. Demco, E. Culea, and B. Blümich, Monte-Carlo Simulations of the Two-Dimensional NMR T_2-T_2 Exchange of Fluids in Porous Media, Diffusion Fundamentals 10 (2009) 20.1 - 20.3.

[48] L. Monteilhet, J.-P. Korb, J. Mitchell, and P. J. McDonald, Observation of exchange of micropore water in cement pastes by two-dimensional T_2-T_2 nuclear magnetic resonance relaxometry, Physical Review E 74, 061404 (2006)

[49] P. J. McDonald, J.-P. Korb, J. Mitchell, and L. Monteilhet, Surface relaxation and chemical exchange in hydrating cement pastes: A two-dimensional NMR relaxation study, Physical Review E 72, 011409 (2005)

[50] P. J. McDonald, Jonathan Mitchell, Michael Mulheron, Luc Monteilhet, Jean-Pierre Korb, Two-dimensional correlation relaxation studies of cement pastes, Magnetic Resonance Imaging, 25, 470–473 (2007).